Robotics and Computer–Integrated Manufacturing 97 (2026) 103063

Contents lists available at ScienceDirect

Robotics and Computer-Integrated Manufacturing

journal homepage: www.elsevier.com/locate/rcim

Full length article

A study on the predictive capabilities of digital twins for object transfers in a remanufacturing demonstration environment

Jan-Felix Klein *, Kai Furmans

Karlsruhe Institute of Technology (KIT), Gotthard-Franz Straße 8, Karlsruhe, 76131, Germany

ARTICLE INFO

Keywords:
Digital twin
Remanufacturing
Cyber-physical system
Object transfer
Material handling
Autonomous mobile robot
Sim-to-real

ABSTRACT

Remanufacturing processes are characterized by high uncertainty due to the variable conditions of returned cores, which makes automation challenging and necessitates considerable process flexibility. Industry 4.0 methods are often proposed to mitigate this uncertainty, yet real-world demonstrations that validate their effectiveness remain limited. This study addresses this research gap by presenting a flexible, digital-twin driven object transfer system implemented in a remanufacturing demonstration environment. The system under consideration involves an autonomous mobile robot that docks at multiple stationary transfer points to transfer unique starter motor cores without the use of load carriers. Since the object transfer process is probabilistic, virtual models are employed in a physics-simulated environment to predict object-specific pre-transfer states, defined as the state an object before the transfer is executed. The predictive capabilities of the digital twins are evaluated through an extensive experimental study, involving a series of physical and virtual experiments conducted on 37 unique starter motor cores.

The study includes calibration experiments to tune the virtual models, followed by large-scale virtual experiments to estimate the probability of successful transfer for a fixed set of pre-transfer states. A custom method is applied to determine the most promising pre-transfer state for each starter motor core. Final validation results highlight the effectiveness of the approach and indicate that increased modeling efforts reveal inherent limitations in the predictive accuracy of the virtual models. Sources of error, including mass distribution approximations and simulation inaccuracies, are discussed, and directions for future improvements are outlined.

1. Introduction

On the road to greenhouse gas neutrality, the common "take, make, waste" approach of the linear production must be transformed into a holistic circular economy that decouples resource consumption from economic growth [1]. Remanufacturing is often considered to be the most superior strategy in terms of overall material and energy savings [2]. Today, remanufacturing is a standardized value retention process in which a remanufactured product is created from restored components of one or more used parts as well as new components. Remanufactured products provide at least the functionality and performance of the original product [3]. The remanufacturing process chain is characterized by a high degree of uncertainty compared to traditional linear production schemes. The inherent uncertainty of the product leads to individual process sequences with highly variable lead times, making it difficult to balance returns and demand [4]. Coping with the variability in quality and quantity requires a high degree of process flexibility at all levels, which until now could only be achieved by a high degree of manual labor with expert knowledge. Researchers generally suggest that increased automation and the implementation of Industry 4.0 methods to reduce costs and improve productivity and quality are potential drivers for the wider application of remanufacturing [5–8]. However, traditional automation methods that rely on a high degree of determinism are not feasible due to the uncertainty inherent in the product and processes. As a result, most research in this area has been conceptual. The lack of real-world demonstrations that show the benefits of applying advanced methods that can cope with uncertainty in remanufacturing is subsequently identified as a research gap [7–9].

We address this gap by presenting a comprehensive experimental study that evaluates the predictive capabilities of digital twins (DTs) for an uncertain object transfer process. The system involves an autonomous mobile robot (AMR) docking at stationary transfer points to transfer unique starter motor cores without the use of load carriers. Virtual models are integrated into the physical system to predict the outcomes of this inherently uncertain transfer process. These predictions enable the system to minimize uncertainty and optimize the

* Corresponding author.
E-mail address: jan-felix.klein@kit.edu (J.-F. Klein).

https://doi.org/10.1016/j.rcim.2025.103063
Received 4 November 2024; Received in revised form 9 May 2025; Accepted 15 May 2025
Available online 5 June 2025

success of the object transfer. This paper presents a condensed version of the experimental study which was previously reported in the author's doctoral dissertation [10].

The paper is organized as follows: Section 2 reviews the literature on the intersections between production logistics, digital twins, remanufacturing and disassembly automation. Section 3 outlines the implemented object transfer system. In Section 4, we introduce the experimental study to evaluate the capabilities of the digital twins. Section 5 summarizes the validation results. Finally, Section 6 concludes the paper and gives an outlook on future research directions.

2. Literature review

This section provides a review on digital twins (DTs) in production logistics and in the context of remanufacturing and disassembly automation [10].

2.1. Digital twins in production logistics

The integration of digital twins in production logistics has gained significant attention due to their potential to enhance efficiency, optimize workflows, and support decision-making in automated material handling. Unlike traditional simulation approaches, DTs enable real-time synchronization between physical and virtual systems, allowing for continuous monitoring and adaptation. Recent literature reviews by [11,12] provide a broad perspective on DT applications in production logistics, identifying key areas such as transportation, packaging, warehousing, material distribution, and information processing.

Several studies demonstrate the practical benefits of DTs in production logistics. [13] illustrate how DTs assist in selecting optimal equipment, such as automated guided vehicles (AGVs), based on simulated path planning. Similarly, [14] discuss their role in AMR and AGV navigation, localization, and safety validation. Virtual modeling has also been applied to conveyor-based systems, as seen in [15,16], where DTs help refine control parameters for reliable material handling.

From a methodological perspective, the implementation of virtual models varies across studies. [11] found that most approaches rely on Discrete Event Simulation (DES), with fewer utilizing physics-based simulations. [17] focus on data synchronization between physical and virtual models in a welding production line, demonstrating the feasibility of DTs in process optimization. These studies collectively highlight the growing role of DTs in production logistics, particularly in automation, real-time monitoring, and predictive decision-making. Research on production logistics for remanufacturing is extremely limited, with only few publications focusing on the material handling challenges specific to automated remanufacturing, see [18,19]. However, addressing these challenges is crucial with respect to the vision of a fully automated remanufacturing facility.

2.2. Digital twins in remanufacturing and disassembly automation

Research on DTs spans a wide range of applications, depending on the scope and level of detail modeled within the virtual counterpart. In the context of remanufacturing and disassembly automation, DTs play a crucial role in handling the inherent variability of returned products, optimizing decision-making, and improving process efficiency. However, the specific research directions within this domain are diverse. To gain a structured understanding of how DTs are currently being explored in remanufacturing and disassembly automation, a systematic literature review was conducted. The selection process is visualized using a PRISMA chart (see Fig. 1), detailing the filtering steps from an initial set of 42 identified records down to a full-text review of 21 relevant studies. The reviewed literature was categorized based on four key characteristics, allowing us to distinguish different research trajectories and technological approaches. The records were structured according to the following four characteristics:

- **Contribution Type**: Contributions in the field of DTs can take various forms. We evaluate the contribution type by assigning one or more of the following aspects: *"Review"*, *"Model"*, *"Product Model"* and *"Algorithm"*.
- **Assets**: The reviewed publications address various physical assets. During the review, we found three main types of assets, namely *"Core"*, *"Waste"* and *"Resources"*. A category encapsulated in brackets refers to a minor contribution to that assets type.
- **Scope**: DTs can be implemented with varying levels of granularity. We differentiate the scope of the DTs into the following categories: *"Life Cycle"*, *"Supply Chain"*, *"Reconditioning"*, *"Disassembly"*, and *"Shop Floor"*.
- **Real-World Demonstration**: The lack of real-world demonstrations of Industry 4.0 methods in remanufacturing is frequently identified as a research gap [7–9]. Therefore, we rate each record based on its real-world demonstration using a scale from "-" to "+++". A "-" indicates no real-world demonstration, while "+++" signifies an extensive application study.

Table 1 shows the classification results based on our analysis. In the following, we briefly discuss each publication. We structured the discussion of the individual records according to the different scopes.

Life cycle

The majority of the reviewed literature focuses on DTs from a life cycle perspective. Wang and Wang propose a system architecture for a digital twin-enabled *Cyber–Physical System* (CPS) and a data model that considers data from the design phase through manufacturing, use phase and recovery over multiple life cycles [20]. An exemplary implementation shows a cloud-based system where core data can be accessed via a web-based front-end by scanning an attached QR code. Tozanali et al. propose a digital twin-based model to estimate an accurate take-back price for a core based on historical data. A discrete event simulation is used to compare different trade-in policies [22]. Wang et al. further provide a holistic architecture that covers multiple product life cycles and attempts to include all stakeholders involved in the remanufacturing process, with the aim of demonstrating a big data application [23]. However, the architecture is highly conceptual and the application scenario as well as the assumption of the potential benefits of applying the architecture are not based on real-world data. Similarly, Zacharaki et al. present the RECLAIM (*REmanufaCturing and Refurbishment LArge Industrial equipment*) architecture of the EU Factory of the Future project [27]. While the holistic architecture is not discussed in greater detail, the publication emphasizes the decision support framework based on a digital twin of the machinery with the aim of optimizing maintenance activities. Wiesner et al. present a data-driven approach to assessing the health of a machine component [33]. For their use case, the authors developed a custom sensor box to predict the remaining time to failure of a spindle bearing. Another architecture with life cycle perspective is proposed by Elsner et al. [34]. The goal of this architecture is to enable dynamic life cycle assessment in the remanufacturing of battery modules. Ke et al. present an intelligent redesign methodology for used products and applies it to clutch case study to find the optimal clutch redesign scheme [35]. Kerin et al. propose a decision making model that optimizes the remanufacturing planning while using data from different stages in a product's life cycle [36]. The authors use a neural network to predict the remaining useful life and a bees algorithm to plan the disassembly sequence. In another publication, Kerin et al. propose a generic product model [37]. After defining the requirements for a product DT, the authors propose a UML class diagram and instantiate it for a single example product.

Supply chain

Three publications examine DTs in the context of remanufacturing from a supply chain perspective. Chen and Huang review the problem of information sharing and examines information asymmetries in remanufacturing supply chains [24]. Guo and Han propose a closed-loop

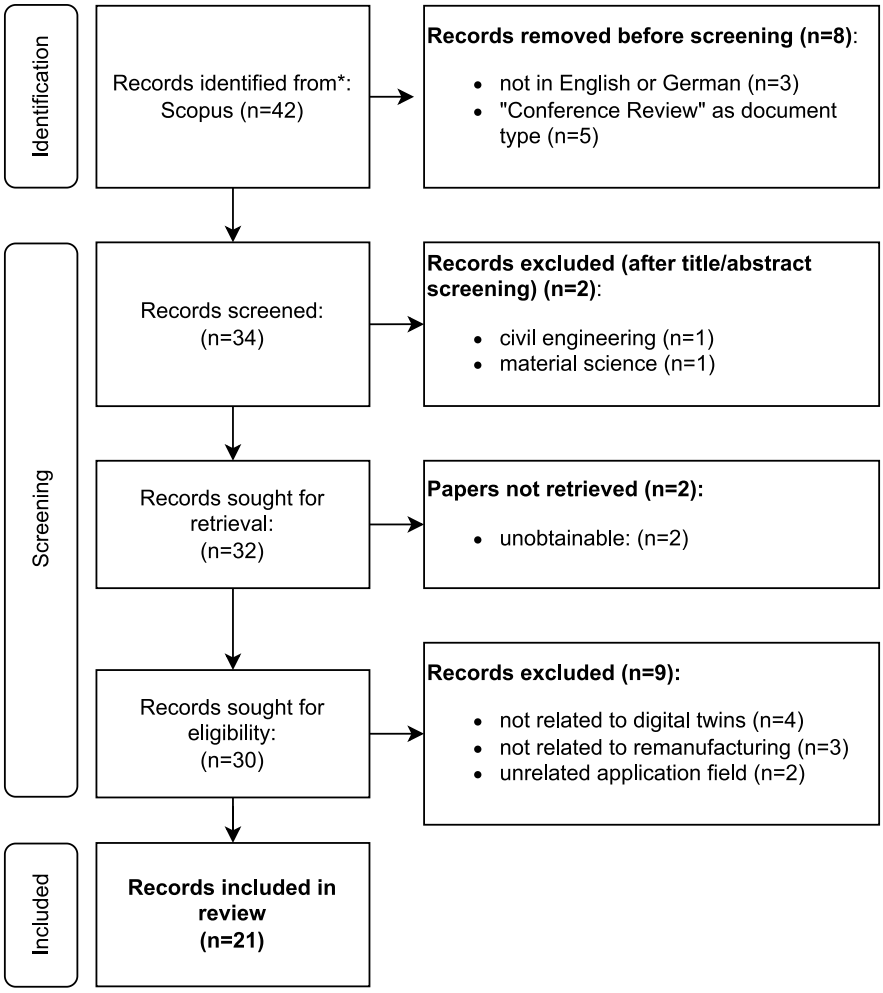

Fig. 1. PRISMA chart of the structured literature review. The records were retrieved from Scopus on the 26th of March 2024 using the query *(digital AND twin*) AND ((remanufactur*) OR (disassembly AND automation))*.

Table 1
Categorized research publications on digital twins in the context of remanufacturing and disassembly automation.

Reference	Contribution type	Assets	Scope	Real-World demonstration
[20]	Architecture, Product Model	Core	Life Cycle	+
[21]	Type	Core, Resources	Disassembly	++
[22]	Model	Core	Life Cycle	–
[23]	Architecture	Core, (Resources)	Life Cycle	–
[24]	Review	Core, Waste	Supply Chain	–
[25]	Analysis	Core, Resources	Reconditioning	–
[26]	Model	Waste	Shop Floor	+
[27]	Architecture	Core, Resources	Life Cycle	–
[28]	Architecture	Core	Shop Floor, Reconditioning	+
[29]	Model, Algorithm	Core	Reconditioning	+
[30]	Model	Core	Supply Chain	–
[31]	Architecture	Core, Resources	Shop Floor	–
[32]	Architecture	Core, Resources	Shop Floor	–
[33]	Model	Core	Life Cycle	+
[34]	Architecture	Core, (Resources)	Life Cycle	–
[35]	Architecture, Model	Core	Life Cycle	+
[36]	Model	Core	Life Cycle,Shop Floor	–
[37]	Product Model	Core	Life Cycle	–
[19]	Architecture, Model	(Core), Resources	Shop Floor	+
[38]	Architecture	(Core), Resources	Supply Chain	+
[39]	Architecture, Model	(Core), Resources	Disassembly	++
This study	Architecture, Model, Algorithm	(Core), Resources	Shop Floor	+++

Table 2
Asset descriptions as used in this study.

Name:	Description
$o^P \in \mathcal{O}^P = \{o_1^P, \dots, o_{37}^P\}$	Physical starter motor core.
TM^P	Physical Transport Module.
$TU^P \in \mathcal{TU}^P = \{TU_A^P, TU_B^P, TU_C^P, TU_D^P\}$	Physical Transfer Unit, one at each of the four stations
$o^V \in \mathcal{O}^V = \{o_1^V, \dots, o_{37}^V\}$	Virtual starter motor core.
$TM^V \in \mathcal{TM}^V$	Virtual instance of a Transport Module.
$TU^V \in \mathcal{TU}^V$	Virtual instance of a Transfer Unit.

digital twin supply chain framework and evaluates the impact of digital twins on the bullwhip effect [30]. Sun et al. propose an architecture for a digital reverse logistics twin in the context of remanufacturing network design [38]. The architecture is evaluated in a case study of a remanufacturing design problem in Norway.

Reconditioning

A further three reviewed publications focus on reconditioning. Shrivastava et al. address the challenges of additive manufacturing in remanufacturing [25]. The authors mention digital twins in combination with other data-driven models as a possible solution to limit the initial process parameter space and reduce of trial-and-error testing. Assuad et al. propose a decision framework for a remanufacturing system based on a laboratory use case, while emphasizing the reconditioning process chain [28]. However, the utility and the interface to specific virtual models of a DT is not further explained. Lastly, Ghorbani and Khameneifar propose a methodology to construct accurate, damage-free digital twins of defective turbine blades and an algorithm to register noisy scanned data to achieve accurate repair volumes for the additive manufacturing process [29].

Disassembly

Rocca et al. provide a comprehensive study of Industry 4.0 technologies in the context of circular economy [21]. The authors developed two simulation models, one to optimize the design of the manufacturing system and a second to optimize the energy consumption during the disassembly process. They also practically demonstrated the capabilities of the DT in a laboratory experiment. Li et al. implemented a human–robot collaboration system and demonstrated the prototype on an electric vehicle battery disassembly task [39]. The system is based on a visual reasoning module that infers task planning strategies while respecting safety and ergonomic rules.

Shop floor

Yang et al. propose a model to dynamically forecast the amount and timing of waste generated during the disassembly process [26]. The model incorporates a digital twin learning loop, in which the model is continuously updated based on new information. The architecture of Hu et al. is the closest to the one presented in the following section [31]. The authors propose a three-layer architecture for a cyber–physical remanufacturing system, consisting of a physical layer, an edge layer and a cloud service layer. In contrast to architecture used in this study, the framework provides an hierarchical approach in which the digital twins are on the edge layer and the logical assets that control the processes are on the top cloud service layer. The proposed architecture by [31] is conceptual only, with no real-world implementation or application provided. Both [19,32] are directly related to this study and are mentioned in the following sections.

As one of the key technologies of Industry 4.0, DTs have received a lot of research attention over the last decade. The inflationary use of the term makes it difficult to provide a consistent definition and to distinguish it from well-known and much older concepts. Most of the research on DTs in remanufacturing and disassembly automation focuses on the life cycle and supply chain perspective. There exist only a few application studies at the shop floor level. As noted in [24] and confirmed by this review, there is only little applied research on digital twins in remanufacturing that has been validated in a real-world application. As indicated in the last row of Table 1, this study contributes to filling this research gap by providing a real-world implementation and an extensive application study to validate the capabilities of DTS of a process that is affected by remanufacturing-specific uncertainties.

3. System overview

This section provides an overview of the system components and processes necessary to understand the experimental study presented in Section 4. For an extensive system description, we refer to [10]. While the challenges outlined here are not directly addressed in this study, their existence underscores the need for digital twins (DTs) to improve the considered object transfer process. The object transfer system considered in this study system was previously introduced in [18,19] and consists of multiple physical and virtual assets, see Table 2. The superscript ^{P} is used throughout this study when referring to the physical assets. The physical object transfer system combines three assets as illustrated in Fig. 2:

- The **Transfer Unit** TU^P is a stationary transfer point that consists of a conveyor belt pair enclosed by two light barriers. The demonstration production system comprises a total of four physical transfer units, see Table 2.
- The **Transport Module** TM^P has an AMR as a base and is equipped with its own transfer unit, see Fig. 2(b). It uses an actuated RGB-D camera to detect and track objects during the object transfer process.
- The **object** to be transferred o^P refers to a unique starter motor core. In this study we consider a total of 37 cores. Fig. 2(g) shows four of these cores. Each core is not only unique in its degree of wear, but originates from a different product variant. The cores share the same product family, which makes them similar in terms of their overall design scheme.

Table 2 shows an overview on all considered assets in this study. For each physical asset, there exists a corresponding virtual model which are referred to using the superscript ^{V}. These were implemented in NVIDIA Isaac Sim, a commonly used physics-based robotic simulation tool based on NVIDIA's physics engine PhysX [40]. Figs. 2(e), 2(f) and 2(h) show instances of the implemented virtual models. The virtual cores are modeled as simple rigid bodies with uniformly distributed mass which use a high resolution STL models as collision shapes. The STL models were generated by scanning the real-world set with a ZEISS T-Scan industrial laser.

3.1. The object transfer process

Fig. 3(a) shows a flowchart of a transport operation, as previously described in [42]. The execution starts with a global navigation process of TM^P targeting a coarse goal position in front of TU^P, see [43] for details. Once TM^P reaches the coarse target pose, the navigation method is switched to a custom laser-based method that uses the cuboid shape of the station modules as a reference to estimate the docking pose. Fig. 3(b) shows an example scenario in which TM^P successfully docked at TU_B^P. Next, the *Object Transfer System* (OTS) is being initiated by TM^P. One can distinguish between two different transfer sequences:

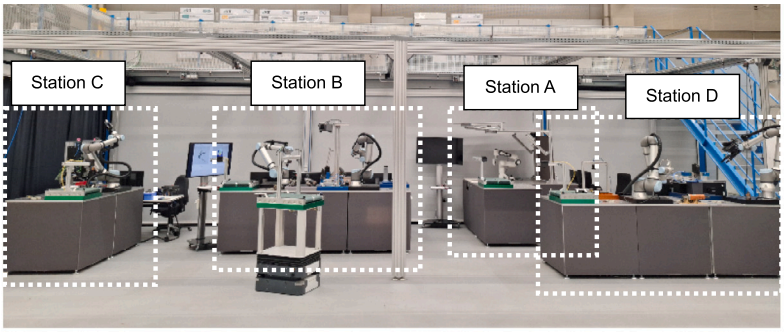

(a) Total view of the *AgiProbot* demonstration production system including four stations and the transport module.

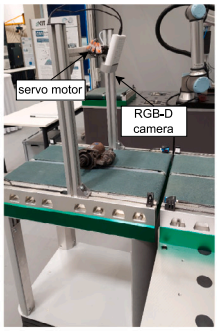

(b) Transport Module.

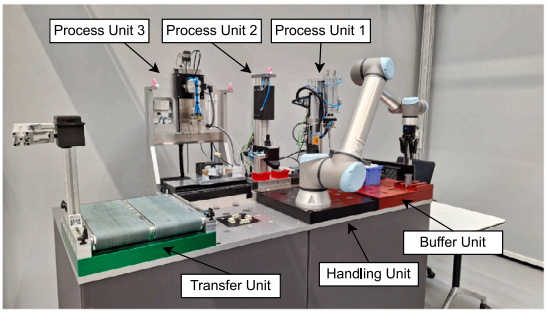

(c) The Transfer Unit as mounted on the *Fluid Automation Station*, see [41].

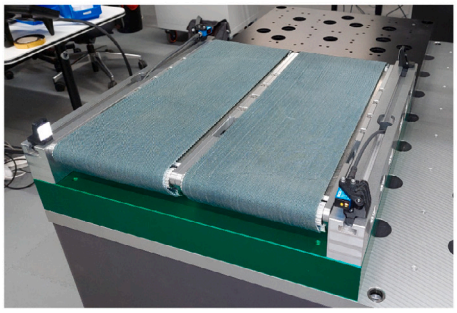

(d) A Transfer Unit: Two separated controlled conveyor belts with two light barriers.

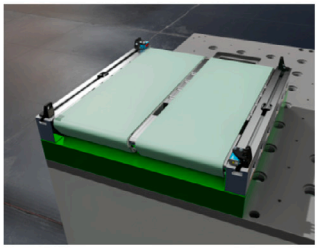

(e) Instance of a virtual transfer unit TU^V

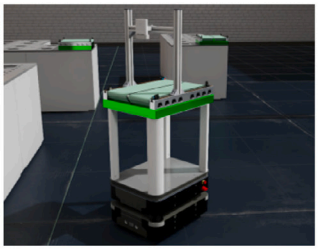

(f) Instance of a virtual transport module TM^V

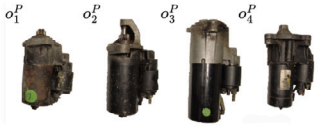

(g) Four physical cores o^P

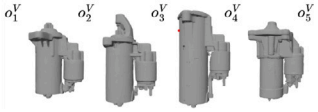

(h) Four virtual cores o^V

Fig. 2. Illustrations of different assets in the *AgiProbot* production system [10]. For additional information on the implemented *Fluid Automation* concept, wee refer to [41].

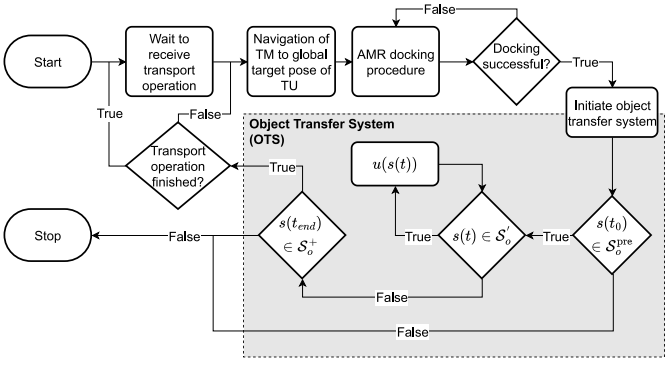

(a) Flowchart of the transport operation execution.

(b) Docked transport module.

Fig. 3. The transport module (TM^P) after a successful docking [10].

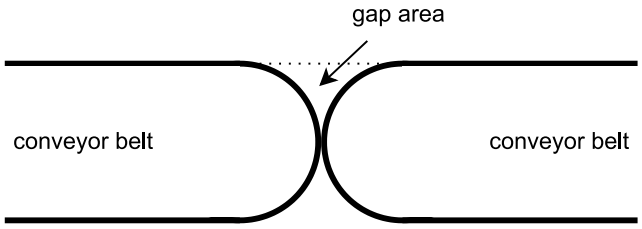

Fig. 4. Gap area between two aligned conveyor belts [10].

- o^P is being transferred from TM^P to TU^P, referred to as a forward transfer.
- o^P is being transferred from TU^P to TM^P, referred to as a backward transfer.

The transfer process operates within a closed-loop control system. An actuated vision system continuously monitors the object's pose while the conveyors run at a constant speed until the object enters a designated goal corridor. Once o^P reaches a pose within this predefined corridor, the OTS concludes, and the transfer is marked as successful. If the object fails to reach the goal corridor within a specified time frame, the transfer is considered unsuccessful.

3.2. Challenges

The object transfer system encounters several challenges that, combined with the uncertainty associated with the transferred cores, may lead to failed transfers. Two key challenges significantly impact the success of the transfer:

- **Object interaction with the conveyor gap**: The object transfer system was designed to transfer a wide variety of objects without requiring containers or other form of load carriers. In principle, two aligned conveyor belts can facilitate a containerless transfer for objects that physically fit within the belts and generate sufficient friction to adopt the linear motion of the rotating belt [44]. When TM^P docks to TU^P, the goal is to position the outer pulleys of the belts as closely as possible without creating physical contact. However, even with perfect alignment, the circular shape of the pulleys create a gap between the flat conveyor surfaces that the objects must overcome during transfer. Fig. 4 shows a side view of the minimum gap area for two perfectly aligned conveyor belts. The object's shape and initial placement on TM^P or TU^P influences its ability to cross the gap. In the worst case, an object may become stuck, preventing a successful transfer.
- **Docking**: The used docking method relies solely on laser data and leverages the cuboid shape of the stations of the considered demonstration environment [43]. The accuracy of the docking pose estimation varies depending on the station module configurations and the location of the transfer unit. After the docking process is completed, a residual docking error remains, which directly impacts the conveyor gap area, further influencing the transfer process.

3.3. Digital twin system

Due to the mentioned challenges, the object transfer process is inherently uncertain, with the success depending on multiple factors. Based on our preliminary study, the following three factors are the most influential [19]:

- The **docking pose quality**: The quality of the docking process directly defines the shape and size of the gap between TM^P and TU^P, see Fig. 4.
- The **object** to be transferred o^P: Since objects are transferred without load carrier, their geometry determines how they interact with the gap between the conveyor belts. Certain shapes may prevent the object from clearing the gap.
- The **pre-transfer object state** s^{pre}: The initial state of o^P on TM^P before the transfer process is being initiated determines how and when different parts of the object interact with the conveyor gap. We call this state the pre-transfer state s^{pre}. A carefully chosen s^{pre} can increase the likelihood of a successful transfer.

To mitigate transfer uncertainty, a digital twin system can be employed, using the previously introduced virtual models to estimate an object-specific s^{pre} that maximizes the probability of success for the given object. Fig. 5 illustrates the system in a runtime scenario. During the diagnosis of a unique core, see [45], virtual OTS instances are generated and initiated using a newly scanned 3D model of the core. These virtual instances simulate different s^{pre} to estimate the optimal one, $s^{\text{pre}}_{\text{best}}$. Once a real-world transfer is requested, the estimated $s^{\text{pre}}_{\text{best}}$ is applied to the physical system. Transfer results for each core are stored in a database, enabling continuous refinement and adaptation for future transfers of the same core or the same core variant. However, a limitation of this approach is the dependency on 3D scanning to generate virtual collision models of each core, which may introduce challenges in large-scale industrial applications. In cases where pre-existing CAD models of the components are available, they could serve as an alternative to reduce the need for scanning each individual part.

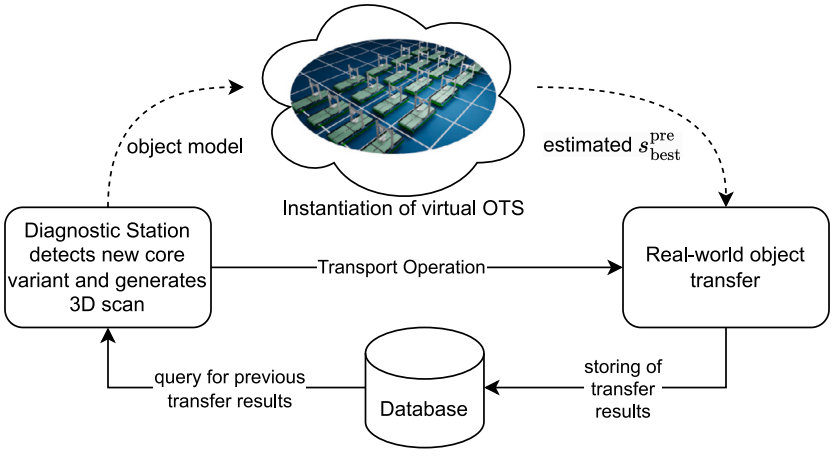

Fig. 5. Workflow of the digital twin system.

Table 3
Overview on the different experiment sets.

Name:	Type	Assets	# repetitions	# unique experiments	# total experiments
Calibration	Physical	$((o^P_1, o^P_{18}, o^P_{23}, o^P_{32}), \mathcal{TM}^P, \mathcal{TU}^P)$	1	4*25	200
Virtual calibration	Virtual	$((o^V_1, o^V_{18}, o^V_{23}, o^V_{32}), \mathcal{TM}^V, \mathcal{TU}^V)$	30	79*200	474.000
Virtual full state	Virtual	$(\mathcal{O}^V, \mathcal{TM}^V, \mathcal{TU}^V)$	50	37*924	1.709.400
Validation	Physical	$(\mathcal{O}^P, \mathcal{TM}^P, \mathcal{TU}^P)$	20	37*2	1480

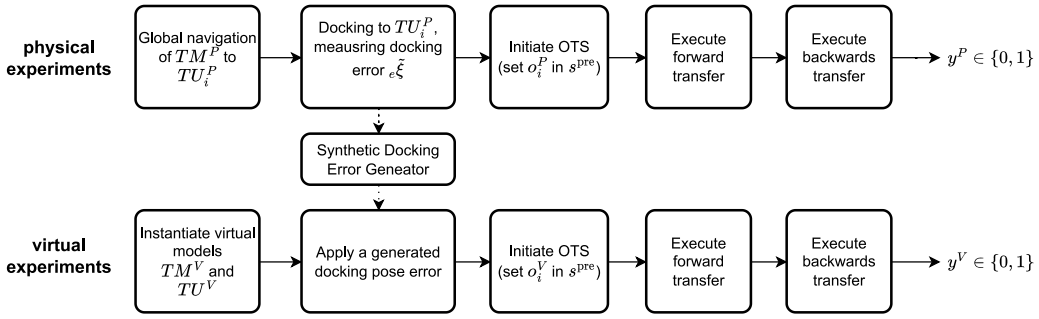

Fig. 6. The procedure of a single object transfer experiment, both for the physical and virtual case.

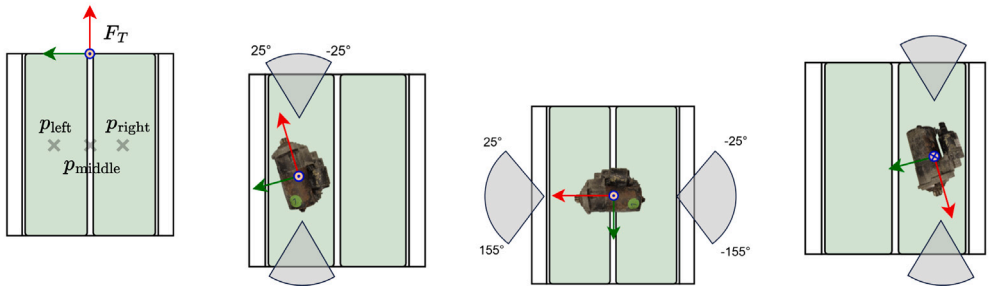

(a) Limited pre-transfer positions (b) $s^{\text{pre}} \in {}^E\mathcal{S}^{\text{pre}}_{\text{left}}$ (c) $s^{\text{pre}} \in {}^E\mathcal{S}^{\text{pre}}_{\text{both}}$ (d) $s^{\text{pre}} \in {}^E\mathcal{S}^{\text{pre}}_{\text{right}}$

Fig. 7. Examples of different pre-transfer states.

4. Experimental study

In general, it is not the effects of a single of these factor, but the combination that determines whether a transfer can be successfully executed or not. The goal of this study is to evaluate the predictive capabilities of our DTs to capture these effects. In general, we use our DTs to predict a single pre-transfer state $s^{\text{pre}}_{\text{best}}$ for each object o^P that maximizes the probability of a successful transfer. To achieve this, we conduct multiple series of experiments in both physical and virtual environments. Fig. 6 illustrates the general procedure of a single experiment in both cases. The experimental study is structured according to the different experiment sets, see Table 3:

1. **Calibration Experiments**: We perform an initial set of physical experiments on a small subset of starter motor cores while measuring the docking pose error.
2. **Virtual Model Calibration**: We use the results of the calibration experiments to tune and parametrize our virtual models. In addition, we use the measured docking pose errors to build a synthetic docking pose generator which allows us to sample realistic docking pose errors for further virtual experiments.
3. **Virtual Full State Experiments**: We conduct a large series of virtual experiments in which we estimate the probability of success $\hat{p}^V$, for each pre-transfer state of each virtual starter motor core o^V.
4. **Determine Best Pre-Transfer State**: Through a series of transformations, we determine s^{pre} for each virtual object o^V. We use this state as an estimate for the corresponding real-world object o^P. To gain additional intuition about the capabilities of our DTs, we similarly determine $s^{\text{pre}}_{\text{worst}}$ which is the state with the lowest probability of success.
5. **Validation**: We validate and compare the results for $s^{\text{pre}}_{\text{best}}$ and $s^{\text{pre}}_{\text{worst}}$ for o^V with o^P by an additional set of real-world experiments.

4.1. Pre-transfer state definition

For the general case, there exists an infinite number of possible pre-transfer states s^{pre} for o^P. For this study, we limit the possible states and define the set of pre-transfer states as follows:

$$\mathcal{S}^{\text{pre}} = \{(\theta, f, c)\} \tag{1}$$

We define θ as the pre-set yaw angle rotation of the object and discretize it to a 1° step size resulting in 360 possible values for θ:

$${}^E\Theta = \{\theta \mid \theta \in \mathbb{Z}, -179 \leq \theta \leq 180\} \tag{2}$$

We further define f, the *face* on which the object is placed on. During initial tests we found that all starter motors, due to their shape, can only be safely placed on either one of two faces:

$$f \in \{\text{'front'}, \text{'back'}\} \tag{3}$$

Figs. 7(b) and 7(c) show the object on the 'front' face, with the engagement relay pointing to the left side with respect to the object's

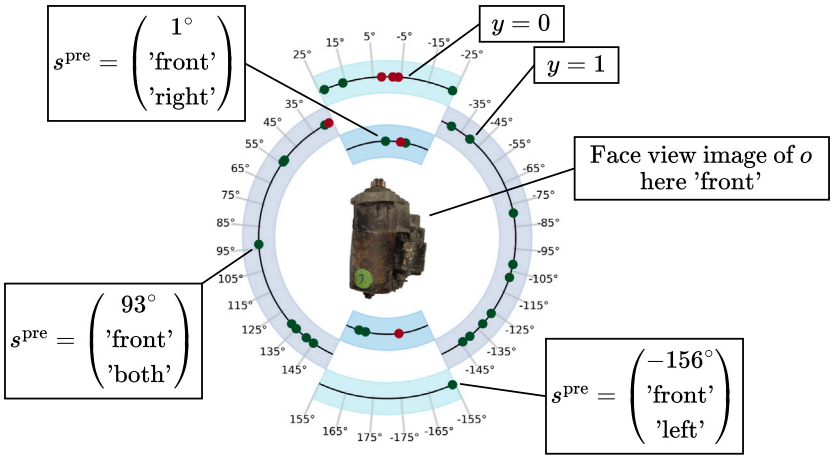

Fig. 8. Exemplary labeled result plot for o_1^P. The greyish center circle refers to results with $\theta \in {}^E\Theta_{\text{both}}$. The blueish small circles cover the possible state space with $\theta \in {}^E\Theta_{\text{single}}$ distinguishing between $c =$ 'left' and $c =$ 'right' [10].

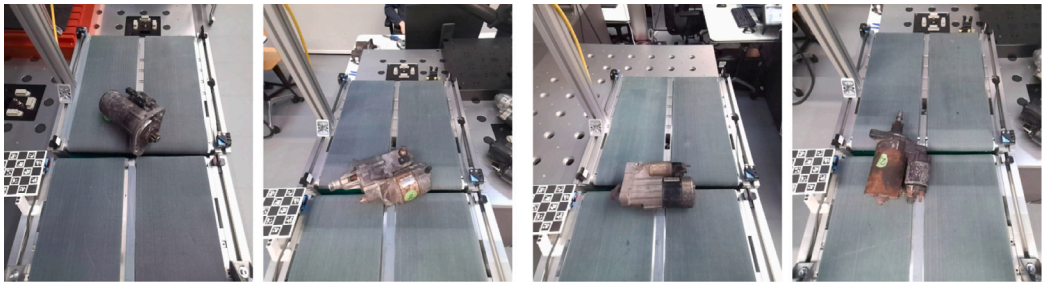

(a) o_1^P with $s^{\text{pre}} = \begin{pmatrix} -52° \\ \text{'back'} \\ \text{'both'} \end{pmatrix}$ (b) o_{18}^P with $s^{\text{pre}} = \begin{pmatrix} 57° \\ \text{'back'} \\ \text{'both'} \end{pmatrix}$ (c) o_{23}^P with $s^{\text{pre}} = \begin{pmatrix} 88° \\ \text{'front'} \\ \text{'both'} \end{pmatrix}$ (d) o_{32}^P $s^{\text{pre}} = \begin{pmatrix} -2° \\ \text{'front'} \\ \text{'left'} \end{pmatrix}$

Fig. 9. Images series of selected *Calibration Experiment* result states: For all selected experiments, the transfer failed. The binary results are also shown in Fig. A.17 [10].

center and the z-axis of the object frame pointing upwards. Fig. 7(d) shows the object on the opposing 'back' face. In addition, we define three different conveyor positions, see Fig. 7(a):

$$c \in \{\text{'left'}, \text{'right'}, \text{'both'}\} \tag{4}$$

Due to size ratio between the conveyor belts and the starter motor cores we do not allow all values of θ for each of the three possible positions c. ${}^E\Theta_{\text{single}}$ defines the value range of θ where we place o^P on a single belt:

$${}^E\Theta_{\text{single}} = [-179.. -155] \cup [-25..25] \cup [155..180] \tag{5}$$

$${}^E\Theta_{\text{both}} = {}^E\Theta \setminus {}^E\Theta_{\text{single}} \tag{6}$$

In total we define a set of **924** possible pre-transfer states:

$${}^E\mathcal{S}^{\text{pre}} = {}^E\mathcal{S}^{\text{pre}}_{\text{left}} \cup {}^E\mathcal{S}^{\text{pre}}_{\text{both}} \cup {}^E\mathcal{S}^{\text{pre}}_{\text{right}} \tag{7}$$

4.2. Calibration experiments

We first perform an initial set of 200 real-world experiments (randomly generated from ${}^E\mathcal{S}^{\text{pre}}$) based on a small subset of four different starter motor cores. These results are further used to parametrize the virtual models. Fig. 8 shows exemplary the results for o_1^P and $f =$ 'front'. Fig. A.17 includes the results for the full set of experiments. We can observe that the results for each core o^P are distinct, presumably due to the unique shapes and the interactions of the shapes with the gap area between the conveyor belts. Overall the real-world calibration experiment results include (135/200) positive examples, $y = 1$ in which the transfer experiment succeeded and (65/200) negative examples, $y = 0$ in which the transfer experiment failed. The majority of the failed object transfers are due to the object not being able to clear the gap between the conveyors, see e.g. the exemplary cases illustrated in Fig. 9. Note that these results are only certain for the specific conditions of the performed experiment, e.g. for a unique docking error of TM^P at TU^P.

Besides determining the object transfer results, we measure the docking error for each object transfer process using stationary cameras on each of the four transfer units and attach a 5 × 5 ChArUco board to TM^P. Fig. 10 shows the measurement results. The histograms of all three components are approximately bell-shaped. For ${}_e\tilde{\xi}_x$ and ${}_e\tilde{\xi}_y$, the values are in an expected range. The histogram of ${}_e\tilde{\xi}_\theta$ is shifted towards positive yaw angle errors. The three docking pose error components are not independent. This can be observed in the 3 × 3 correlation matrix as shown in Fig. 10(b) with the largest correlation between the x-translation and the y-translation.

4.3. Virtual model calibration

To mimic the docking error for our virtual model, we train a *Synthetic Docking Error Generator* based on the 200 measured docking errors as described in the previous section. Due to the dependencies between each docking error component, the synthesizer must be able to capture the joint distribution. To achieve this, we use the *Synthetic Data Vault*, an open source framework for training generative models based on tabular data [46]. We achieved the best results by using the Gaussian Copula model which can be used to describe the dependence structure

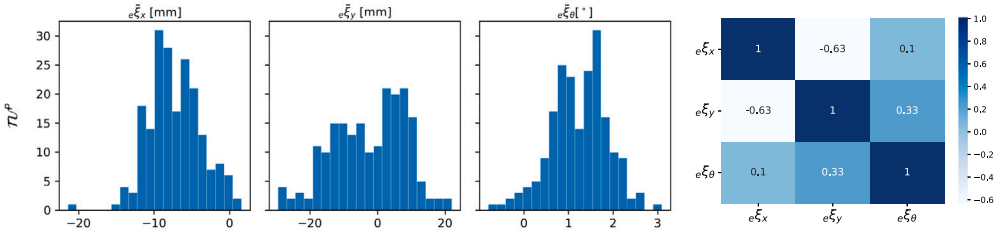

(a) Histogram (b) Correlation matrix.

Fig. 10. Docking error measurement results [10].

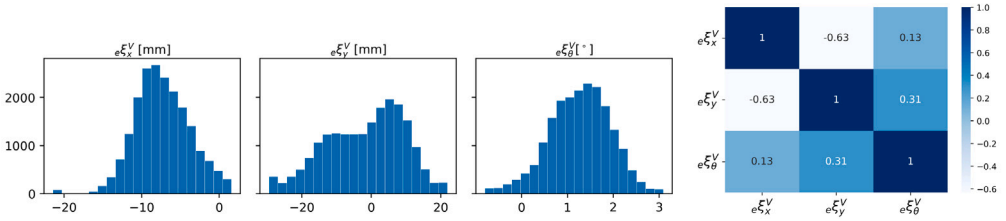

(a) Histogram of 20000 synthetic generated docking pose errors (b) Synthetic correlation matrix

Fig. 11. Synthetically generated docking pose errors [10].

Table 4
Metrics of a single series of 30 *Virtual Calibration Runs* with the final selected parameter set [10].

PP	PN	FP	FN	TP	TN	Accuracy	Precision	Recall	$F_{0.5}$
123.5	**76.5**	**18.0**	**29.5**	**105.5**	**47.0**	**0.7627**	**0.8548**	**0.7815**	**0.8389**
±4.3	±4.3	±2.8	±3.1	±3.1	±2.8	±0.021	±0.019	±0.023	±0.017

between random variables while preserving their marginal distributions. Fig. 11 shows a corresponding histogram and its correlation matrix. As shown in Table 3, we performed a set of *Virtual Calibration Experiments* in which we simulate the 200 calibration experiments as introduced previously while we vary different simulation parameters. Due to the inherently non-deterministic behavior of physics engines, we cannot rely on the results of a single run for a given parameter set. To obtain reliable results it therefor essential to perform each run several times (we perform 30 repetitions) and analyze the distribution of the results. We treat the comparison between a *Virtual Calibration Run* and the corresponding real-world experiments as a binary classification problem. We use the $F_{0.5}$ score as our main metric to evaluate the fit since we want to ensure that the virtual models are tuned more conservatively, as more emphasis on precision reduces the number of false positives.

We divided the tuning process into a two-step process. We first evaluated the influence of 9 physics-engine specific parameters and afterwards optimized for two use-case specific parameters, namely the *Dynamic Friction Coefficient* and the *Initial Gap Distance*, the initial distance between the docked conveyors before applying a synthetic docking error.

Table 4 shows the numerical results for our best performing parameter set. We obtain a mean score of $F_{0.5} \approx 0.84$ with a higher precision than recall, indicating a more conservative model. This is underlined by the number of *False Positives* (FP) being lower then the *False Negatives* (FN). The accuracy is still reasonably high (≈ 0.76), suggesting that the virtual models are performing well overall in simulating object transfers.

4.4. Virtual full state experiments

Using the calibrated virtual models, we perform an extended series which we refer to as the *Virtual Full State Experiments*. In this series, we simulate the object transfer experiments of each o^V for each of the 924 pre-transfer state and repeat each experiment 50 times, see Table 3. At each repetition we sample and apply a new docking error from our synthetic docking error generator, which subsequently leads to different results in each run even though all other inputs are kept constant (including s^{pre}).

For the post-processing steps, we separate the results for each o^V into four results sets. Each of these sets include 360 pre-transfer states (full object rotation), but differ in their positions on the conveyor belt (c and f values):

$$ {}^E\mathcal{S}^{\text{pre}}_{\text{front,left}} = \left\{ s \in {}^E\mathcal{S}^{\text{pre}} \;\middle|\; \begin{pmatrix} f = \text{'front'} \\ c = \{\text{'both'}, \text{'left'}\} \end{pmatrix} \right\} \tag{8} $$

We define ${}^E\mathcal{S}_{\text{front,right}}$, ${}^E\mathcal{S}_{\text{back,left}}$ and ${}^E\mathcal{S}_{\text{back,right}}$ accordingly. For each of these sets we can visualize the results as a binary series over θ. Fig. 12(a) visualizes the exemplary results for o^V_1 for the pre-transfer set ${}^E\mathcal{S}_{\text{front,right}}$. Fig. 12(b) shows the processed results after calculating the mean values $\overline{Y}$ over all runs.

Before determining $s^{\text{pre}}_{\text{best}}$, we apply a centered moving average filter to the mean values $\overline{Y}$. Smoothing the results using this filter has several practical implications:

- The calibration experiment results of Table 4 indicate the presence of a sim-to-real gap which limits the overall prediction accuracy. Therefore, rather than relying on a single local optimum, we prioritize a range of states with high probability.
- A broader range of neighboring states (in terms of θ) with high values for $\overline{y}^V$ suggests that the real probability for the given state is indeed high.
- In real-world scenarios, a handling robot, which is controlled to place o^P in a proposed pre-transfer state may not achieve the required accuracy to place the object exactly in a specific state s^{pre}.

We denote the filtered results as $\overline{Y}^{MA}$. Fig. 12(c) shows the results after applying it. We perform the steps on all four result subsets leading to

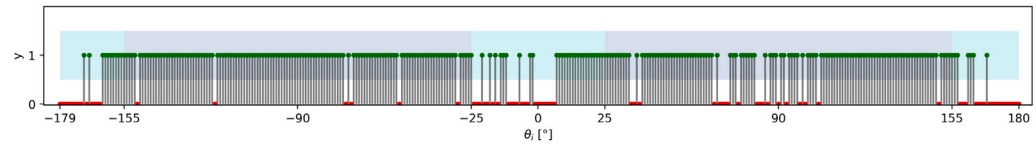

(a) Binary results for a single *Full State Run*: $Y_{o_1^V,1,\text{front,left}}$

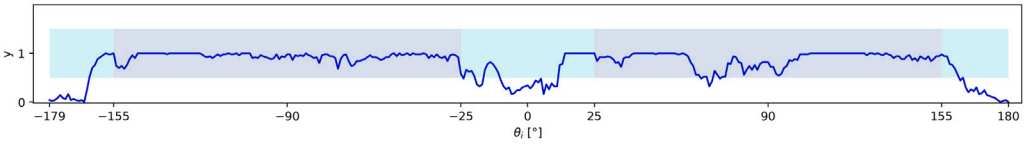

(b) Mean transfer results $\overline{Y}_{o_1^V,\text{front,left}}$. based on 50 repetitions.

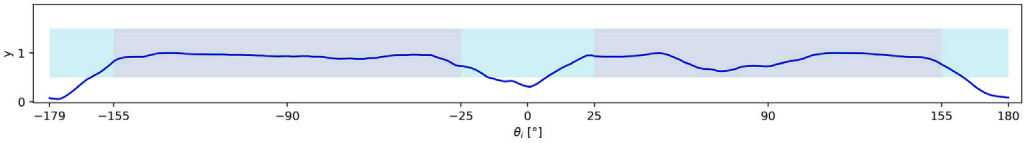

(c) Results with applied moving average filter $\overline{Y}^{MA}_{o_1^V,\text{front,left}}$.

Fig. 12. Post-Processing steps on the binary transfer results. The results are visualized as the binary outcome over θ. The background colors match with the colors introduced in Fig. 8 [10].

the overall post-processed results:

$$Y = \{\overline{Y}^{MA}_{\text{front,left}}, \overline{Y}^{MA}_{\text{front,right}}, \overline{Y}^{MA}_{\text{back,left}}, \overline{Y}^{MA}_{\text{back,right}}\} \tag{9}$$

4.5. Determining best pre-transfer states

We use the following two-step approach to determine $s^{\text{pre}}_{\text{best}}$ and $s^{\text{pre}}_{\text{worst}}$ for each object o^V:

1. We first determine the best local state for each data series $\overline{Y}^{MA} \in Y$, see algorithms 1 and 3 respectively. Given a single result series $\overline{Y}^{MA} \in Y$, we first filter for all states that share the maximum value of $\overline{y}^{MA}$. Taking the example plot for o_1^V in Fig. 13(a), several states were estimated with $\overline{y}^{MA} = 1$. If only a single state has the maximum value, we found $s^{\text{pre}}_{\text{best}}$ already. If multiple states share this value, we again perform a moving average filter on each of the candidates. In the next iteration, we increase the window size and only keep the states with the highest results after applying the filter. We end up with a single state $s^{\text{pre}}_{o,\text{best}}$ which not only has the highest value for $\overline{y}^{MA}_i$ but also the most neighboring states with equally high values.
2. We use the results in algorithms 2 and 4 respectively to determine the global $s^{\text{pre}}_{\text{best}}$ and $s^{\text{pre}}_{\text{worst}}$. We compare the four candidates from each result subset and select the one with the highest value of $\overline{y}^{MA}$ and, if multiple states share this value, we select the one with the highest value of the applied window size in the previous step. The star in Fig. 13 indicates determined $s^{\text{pre}}_{\text{best}}$, the red cross indicates $s^{\text{pre}}_{\text{worst}}$.

Fig. C.18 shows the result plots for all $o^V \in \mathcal{O}^V$. The plots show unique results for each of the objects which demonstrates the complexity and difficulty in predicting the behavior of each individual starter motor core during an object transfer.

5. Validation and discussion

To validate the predictions, an additional series of real-world experiments is performed which is called *Validation Experiments*, see Table 3. In the previous section, $\overline{y}^V$ was determined for both pre-transfer states $s^{\text{pre}}_{\text{best}}$ and $s^{\text{pre}}_{\text{worst}}$ as the mean result of binary object transfer experiments. Since each repetition is statistically independent, one can treat $\overline{y}^V$ as an estimate of the probability of success ($\hat{p}^V = \overline{y}^V$) and the repeated object transfer experiments as Bernoulli trials. The Clopper–Pearson interval [47] is used to calculate the confidence intervals for these bernoulli trials, which is considered to be a rather conservative method of calculating the confidence interval for a binomial distribution [48]. Fig. 14 shows the resulting 95% confidence intervals for the *Validation Experiments* (black intervals) and the corresponding virtual *Virtual Full State Experiments* (blue intervals) for $s^{\text{pre}}_{\text{best}}$ for each o^P and o^V.

One can observe that most of the selected $s^{\text{pre}}_{\text{best}}$ have $\hat{p}^V \simeq 1$, with few exceptions, e.g. o^V_{36} has only a medium high probability of success ($\hat{p}^V = 0.52$) suggesting that the object is generally difficult to transfer. To compare the confidence intervals, the *Newcombe Hybrid Score* confidence interval is used [49] for the difference ($\hat{p}^V - \hat{p}^P$), one of the recommended methods by [50] for comparing the results of two independent Bernoulli experiments. For (12/37) objects a significant difference between the confidence intervals between the virtual and the real results exists. In Fig. 14, these objects were marked with a red background color in their respective columns.

Similarly, Fig. 15 shows the resulting 95% confidence intervals for $s^{\text{pre}}_{\text{worst}}$ for each $o \in \mathcal{O}$. For the majority of objects, $s^{\text{pre}}_{\text{worst}}$ has a probability of success $\hat{p}^V \simeq 0$. This indicates that for this particular pre-transfer state, the object cannot be successfully transferred by the DTs. Some objects, e.g. $o^V_{19}, o^V_{23}, o^V_{25}$ or o^V_{28} have considerable higher probabilities for $s^{\text{pre}}_{\text{worst}}$. The object o^V_{28} has a probability of $\hat{p}^V = 1.0$ for its worst state. This indicates that the object could be successfully be transferred by the DTs for all of its pre-transfer states. When comparing the results for $s^{\text{pre}}_{\text{worst}}$, (17/37) objects have significant different confidence intervals for the virtual and the physical results. The overall results suggest some sources of error that prevent the DTs from estimating the transfer probabilities more accurately. These errors can be either:

- asset-related, meaning that the virtual models of the transport module, transfer unit or the considered objects do not sufficiently model the real system,
- or physics-engine related, meaning that the engine is either not sufficiently calibrated or in general not sufficient enough to capture the physical interaction during the object transfers.

Defining the exact reason for each individual case is a difficult task as many errors may overlap and lead to the individual results. In

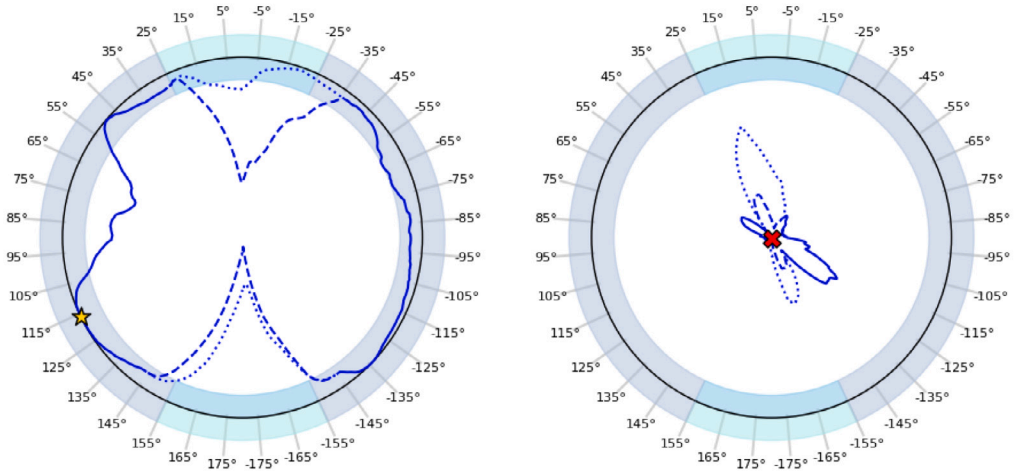

(a) $\{\overline{Y}^{MA}_{o_1^V,\text{front,left}}, \overline{Y}^{MA}_{o_1^V,\text{front,right}}\}$: The yellow star indicates $s^{\text{pre}}_{\text{best}}$

(b) $\{\overline{Y}^{MA}_{o_1^V,\text{back,left}}, \overline{Y}^{MA}_{o_1^V,\text{back,right}}\}$: The red cross indicates $s^{\text{pre}}_{\text{worst}}$

Fig. 13. Virtual full state experiment results for o_1^V including $s^{\text{pre}}_{\text{best}}$ and $s^{\text{pre}}_{\text{worst}}$ determined for [10].

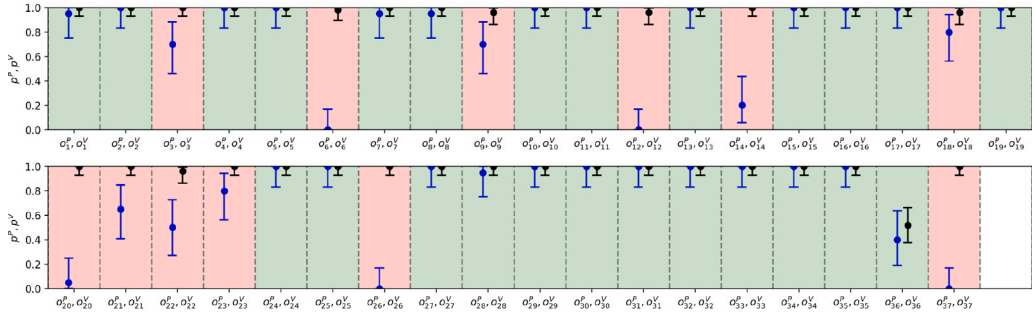

Fig. 14. Confidence interval comparison between virtual and physical results for $s^{\text{pre}}_{\text{best}}$.

the following, we give three implications for sources of error using examples from the *Validation Experiments*:

- **Mass Distribution Approximation**: The virtual object models are all approximated with a uniform mass distribution across the collision volume. This approximation does not accurately reflect the true mass distribution of the objects, leading to incorrect calculations of forces and during the transfer process. For the object transfer example, the real objects may have different contact points during the process compared to the virtual one. For some objects, we can observe this difference in the distribution of mass already during the pre-transfer state. Figs. 16(a) and 16(b) visualize two cases for o_{14} and o_{22}.
- **Unstable Physics Simulation**: We are experiencing issues with the physics engine during some object transfers, where objects are unexpectedly catapulted into the air. This problem occurs when the physics simulation fails to correctly handle the contact transition, causing objects to experience excessive and unintended forces, disrupting the expected behavior and stability of the simulation. We have observed this issue for $s^{\text{pre}}_{\text{worst}}$ for objects o_6^V, o_{17}^V and o_{22}^V. Figs. 16(i) and 16(j) show two examples for o_6^V and o_{17}^V.
- **Inaccurate Collision Shapes**: We have observed two cases, where the virtual (scanned) model of the starter motor core is inaccurate, see Figs. 16(c)–16(h). o_{18}^P has an elastic part, which is rigid for the scanned virtual model o_{18}^V, see Fig. 16(c). For $s^{\text{pre}}_{o,\text{best}}$, this affects the contact points during the object transfer process. o_{24}^P has a cable tie that was included in the scan which results in it being rigid in the collision model.

In summary, while the estimates of the DTs are promising, further modeling efforts, particularly in refining the virtual environment and the virtual models, could enhance prediction accuracy. However, the tradeoff between additional modeling efforts and the marginal improvements must be carefully considered. Additionally, future studies could examine how incorporating prior object knowledge, e.g. accurate pre-known mass distributions, affects the estimation results.

6. Conclusion and outlook

This work illustrated an object transfer system, developed as part of a remanufacturing demonstration environment and designed to transfer unique starter motor cores between different stations. The system

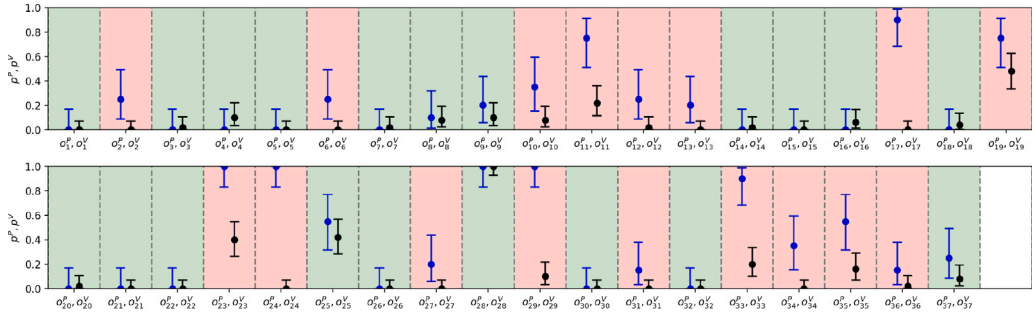

Fig. 15. Confidence interval comparison between virtual and physical results for $s^{\text{pre}}_{\text{worst}}$ [10].

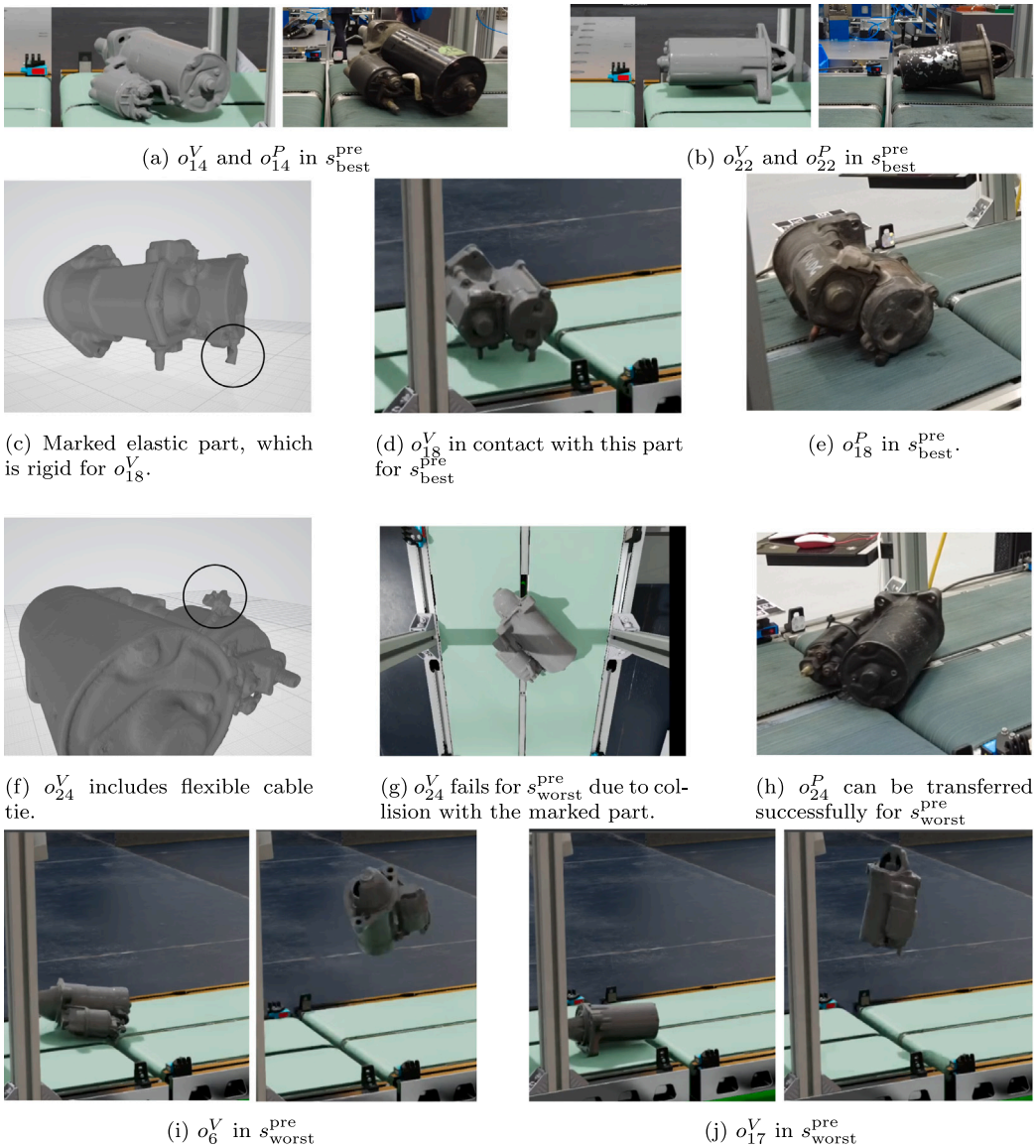

(a) o^V_{14} and o^P_{14} in $s^{\text{pre}}_{\text{best}}$

(b) o^V_{22} and o^P_{22} in $s^{\text{pre}}_{\text{best}}$

(c) Marked elastic part, which is rigid for o^V_{18}.

(d) o^V_{18} in contact with this part for $s^{\text{pre}}_{\text{best}}$

(e) o^P_{18} in $s^{\text{pre}}_{\text{best}}$.

(f) o^V_{24} includes flexible cable tie.

(g) o^V_{24} fails for $s^{\text{pre}}_{\text{worst}}$ due to collision with the marked part.

(h) o^P_{24} can be transferred successfully for $s^{\text{pre}}_{\text{worst}}$

(i) o^V_6 in $s^{\text{pre}}_{\text{worst}}$

(j) o^V_{17} in $s^{\text{pre}}_{\text{worst}}$

Fig. 16. Examples for errors sources: inaccurate mass distributions lead to a different set of contact points (16(a), 16(b)), physical twins include flexible parts (16(c)–16(h)) and unstable physics simulation leading to launching virtual object models after entering the conveyor gap (16(i), 16(j)) [10].

integrates a freely moving transport module based on an autonomous mobile robot, with multiple stationary transfer units that serve as the physical receivers for the starter motor cores. The focus of this study was on the implemented digital twins (DTs) of the object transfer system. Due to the inherent uncertainty with regards to the varying shapes of the starter motor cores, the object transfer process must be considered probabilistic. The DTs are therefore being used to mitigate the uncertainty by suggesting an object-specific pre-transfer state that maximizes the probability of a successful transfer. The pre-transfer state, which defines object's physical state before the transfer is initiated, serves as a controllable parameter and can be adjusted, for instance, using a handling robot.

In our experimental study, which considered 37 unique starter motor cores, we conducted multiple series of physical and virtual experiments to evaluate the predictive capabilities of the developed DTs. Based on a small set of physical calibration experiments, the virtual models of the DTs were tuned, resulting in a mean score $F_{0.5} \approx 0.84$ for the best parameter combination found. The tuned models were then used to estimate the probability of success for different pre-transfer states of each individual cores. Based on these estimates, we proposed a method to determine the pre-transfer states with the highest and lowest probability of success which were subsequently validated in an additional set of real world experiments. For the best states, 12 out of 37 objects showed significant differences between the virtual and real-world results based on the calculated confidence intervals, while for the worst states, 17 out of 37 objects showed similar discrepancies.

Several sources of error were discussed, including approximations in mass distribution, instabilities in the physics simulation and inaccurate collision shapes. Future research could further explore the impact of increased modeling effort related to the virtual environment and the virtual models on the prediction results while evaluating the generalization to different types of cores. Additionally, further integration is required to fully incorporate the DTs' predictive capabilities into the runtime system of the production control. This would enable the evaluation of the effectiveness of the DTs in terms of factory-level KPIs. In this study, we focused on the implementation of a single, specific object transfer system. In the future, related uncertain object transfer scenarios (including, e.g., handling operations with a manipulator) could be evaluated similarly.

CRediT authorship contribution statement

Jan-Felix Klein: Writing – review & editing, Writing – original draft, Visualization, Validation, Software, Resources, Project administration, Methodology, Investigation, Funding acquisition, Formal analysis, Data curation, Conceptualization. **Kai Furmans:** Writing – review & editing, Supervision, Funding acquisition, Conceptualization.

Declaration of competing interest

The authors declare the following financial interests/personal relationships which may be considered as potential competing interests: Jan-Felix Klein reports financial support, equipment, drugs, or supplies, and travel were provided by German Research Foundation. If there are other authors, they declare that they have no known competing financial interests or personal relationships that could have appeared to influence the work reported in this paper.

Acknowledgment

Funded by the Deutsche Forschungsgemeinschaft (DFG, German Research Foundation) – SFB 1574 – 471687386

Appendix A. Calibration experiment results

See Fig. A.17.

Appendix B. Algorithms

Algorithm 1 Find Best Pre-Transfer State (Local)

Input: Single result set $\overline{Y}^{MA} \in Y_{o^V}$, see Eq. (9).
Output: BestStateLocal, AppliedHalfWindowSize
MaxValue $\leftarrow -\infty$
MaxEntries $\leftarrow \emptyset$
for each $(\overline{y}^{MA}, \theta) \in \overline{Y}^{MA}$ **do**
  if $\overline{y}^{MA}$ > MaxValue **then**
    MaxValue $\leftarrow \overline{y}^{MA}$
    MaxEntries $\leftarrow \{(\overline{y}^{MA}, \theta)\}$
  else if $\overline{y}_i^{MA}$ = MaxValue **then**
    Add $(\overline{y}_i^{MA}, \theta_i)$ to MaxEntries
  end if
end for
HalfWindowSize $\leftarrow 1$
while |MaxEntries| > 1 **do**
  MaxFilteredValue $\leftarrow -\infty$
  FilteredEntries $\leftarrow \emptyset$
  for each $(\overline{y}^{MA}, \theta) \in$ MaxEntries **do**
    Apply moving average filter on initial set $\overline{Y}^{MA}$
    FilteredValue $\leftarrow \frac{1}{\text{HalfWindowSize}*2+1} \sum_{j=-\text{HalfWindowSize}}^{\text{HalfWindowSize}} \overline{y}_{i+j}^{MA}$
    if FilteredValue > MaxFilteredValue **then**
      MaxFilteredValue $\leftarrow$ FilteredValue
      FilteredEntries $\leftarrow \{(\overline{y}^{MA}, \theta)\}$
    else if FilteredValue = MaxFilteredValue **then**
      Add $(\overline{y}_i^{MA}, \theta_i)$ to FilteredEntries
    end if
  end for
  MaxEntries $\leftarrow$ FilteredEntries
  HalfWindowSize $\leftarrow$ HalfWindowSize + 1
end while
assert |MaxEntries| = 1
BestStateLocal $\leftarrow$ MaxEntries[1]
AppliedHalfWindowSize $\leftarrow$ HalfWindowSize[1]

Algorithm 2 Find Best Pre-Transfer State (Global)

Input: Full result set Y_{o^V}, see Eq. (9).
Output: BestStateGlobal
BestStateGlobal $\leftarrow (-1, -1)$ ▷ Initialize BestStateGlobal with a placeholder
MaxValueGlobal $\leftarrow -\infty$
MaxHalfWindowSize $\leftarrow 0$
for all $\overline{Y}^{MA} \in Y_{o^V}$ **do**
  LocalResult $\leftarrow$ Call Algorithm 1 with $\overline{Y}^{MA}$ as input .
  BestStateLocal $\leftarrow$ LocalResult[1]
  AppliedHalfWindowSize $\leftarrow$ LocalResult[2]
  if BestStateLocal[1] > MaxValueGlobal **then**
    BestStateGlobal $\leftarrow$ BestStateLocal
    MaxHalfWindowSize $\leftarrow$ AppliedHalfWindowSize
  else if BestStateLocal[1] = BestStateGlobal **then**
    if AppliedHalfWindowSize > MaxHalfWindowSize **then**
      BestStateGlobal $\leftarrow$ BestStateLocal
      MaxHalfWindowSize $\leftarrow$ AppliedHalfWindowSize
    end if
  end if
end for

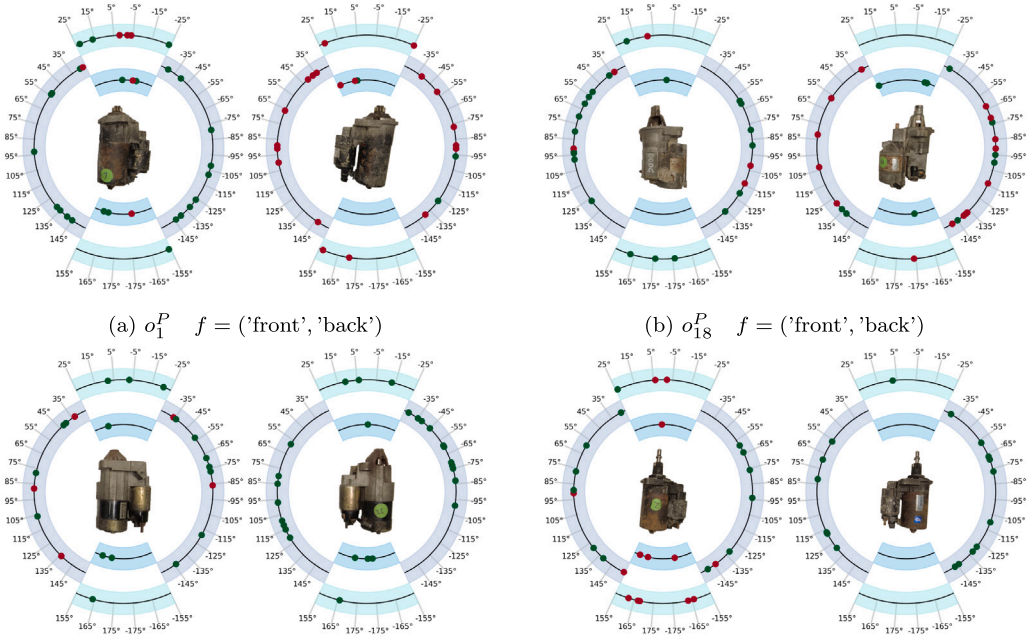

(a) $o_1^P \quad f = (\text{'front'}, \text{'back'})$ (b) $o_{18}^P \quad f = (\text{'front'}, \text{'back'})$

(c) $o_{23}^P \quad f = (\text{'front'}, \text{'back'})$ (d) $o_{32}^P \quad f = (\text{'front'}, \text{'back'})$

Fig. A.17. Real world experiment results for four different starter motor core variants $\{o_1^P, o_{18}^P, o_{23}^P, o_{32}^P\}$. Each subfigure shows the results for (f = 'front') on the left and (f = 'back') on the right [10].

Algorithm 3 Find *Worst* Pre-Transfer State (Local)

Input: Single result set $\overline{Y}^{MA} \in Y_{o^V}$, see Eq. (9).
Output: WorstStateLocal, AppliedHalfWindowSize
  MinValue $\leftarrow \infty$
  MinEntries $\leftarrow \emptyset$
  for each $(\overline{y}^{MA}, \theta) \in \overline{Y}^{MA}$ **do**
    if $\overline{y}^{MA} <$ MinValue **then**
      MinValue $\leftarrow \overline{y}^{MA}$
      MinEntries $\leftarrow \{(\overline{y}^{MA}, \theta)\}$
    else if $\overline{y}^{MA} =$ MinValue **then**
      Add $(\overline{y}^{MA}, \theta)$ to MinEntries
    end if
  end for
  HalfWindowSize $\leftarrow 1$
  while |MinEntries| > 1 **do**
    MinFilteredValue $\leftarrow \infty$
    FilteredEntries $\leftarrow \emptyset$
    for each $(\overline{y}^{MA}, \theta) \in$ MinEntries **do**
      Apply moving average filter on initial set $\overline{Y}^{MA}$
      FilteredValue $\leftarrow \frac{1}{\text{HalfWindowSize}*2+1} \sum_{j=-\text{HalfWindowSize}}^{\text{HalfWindowSize}} \overline{y}_{i+j}^{MA}$
      if FilteredValue $<$ MinFilteredValue **then**
        MinFilteredValue $\leftarrow$ FilteredValue
        FilteredEntries $\leftarrow \{(\overline{y}^{MA}, \theta)\}$
      else if FilteredValue $=$ MinFilteredValue **then**
        Add $(\overline{y}^{MA}, \theta)$ to FilteredEntries
      end if
    end for
    MinEntries $\leftarrow$ FilteredEntries
    HalfWindowSize $\leftarrow$ HalfWindowSize $+ 1$
  end while
  assert |MinEntries| $= 1$
  WorstStateLocal $\leftarrow$ MinEntries[1]
  AppliedHalfWindowSize $\leftarrow$ HalfWindowSize[1]

Algorithm 4 Find *Worst* Pre-Transfer State (Global)

Input: Full result set Y_{o^V}, see Eq. (9).
Output: WorstStateGlobal
  WorstStateGlobal $\leftarrow (-1, -1)$ ▷ Initialize WorstStateGlobal with a placeholder
  MinValueGlobal $\leftarrow \infty$
  MinHalfWindowSize $\leftarrow 0$
  for all $\overline{Y}^{MA} \in Y_{o^V}$ **do**
    LocalResult $\leftarrow$ Call Algorithm 3 with $\overline{Y}^{MA}$ as input .
    WorstStateLocal $\leftarrow$ LocalResult[1]
    AppliedHalfWindowSize $\leftarrow$ LocalResult[2]
    if WorstStateLocal[1] $<$ MinValueGlobal **then**
      WorstStateGlobal $\leftarrow$ WorstStateLocal
      MinHalfWindowSize $\leftarrow$ AppliedHalfWindowSize
    else if WorstStateLocal[1] $=$ WorstStateGlobal **then**
      if AppliedHalfWindowSize $<$ MinHalfWindowSize **then**
        WorstStateGlobal $\leftarrow$ WorstStateLocal
        MinHalfWindowSize $\leftarrow$ AppliedHalfWindowSize
      end if
    end if
  end for

Appendix C. Virtual full state experiments results

See Fig. C.18.

Data availability

Data will be made available on request.

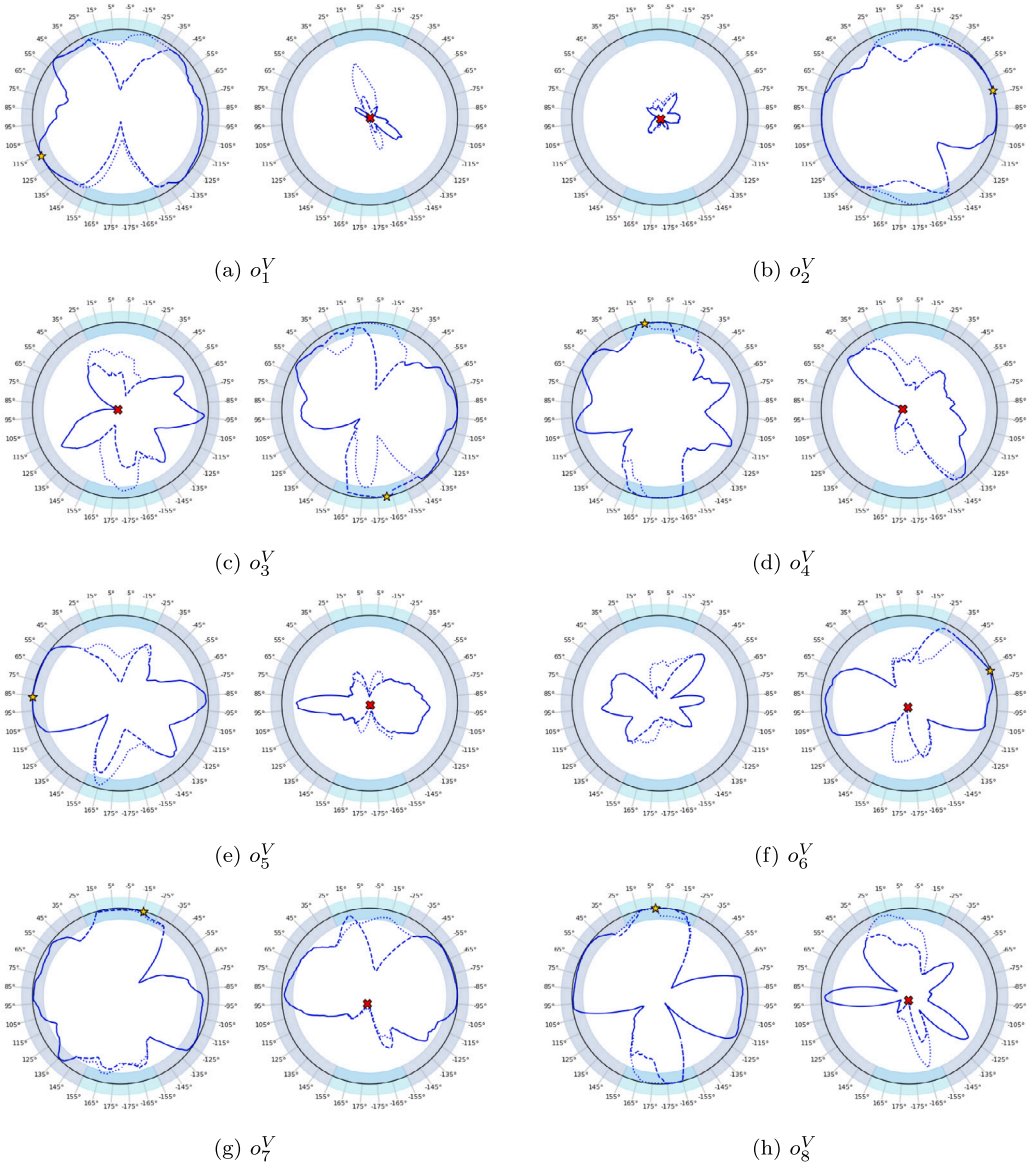

(a) o_1^V (b) o_2^V

(c) o_3^V (d) o_4^V

(e) o_5^V (f) o_6^V

(g) o_7^V (h) o_8^V

Fig. C.18. Virtual full state experiment results Y_{o^V} for each $o^V \in \mathcal{O}^V$ [10].

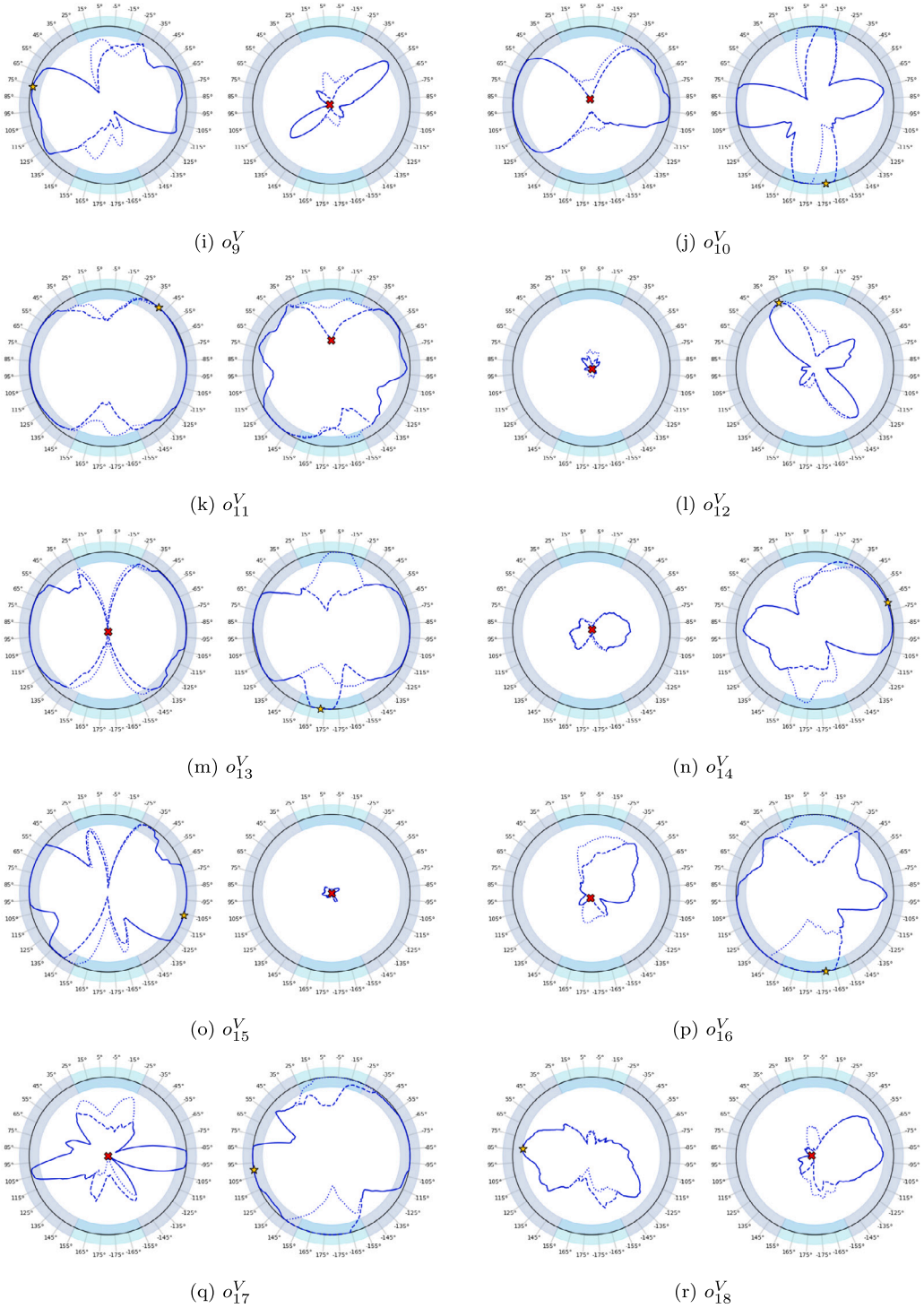

(i) o_9^V (j) o_{10}^V

(k) o_{11}^V (l) o_{12}^V

(m) o_{13}^V (n) o_{14}^V

(o) o_{15}^V (p) o_{16}^V

(q) o_{17}^V (r) o_{18}^V

Fig. C.18. (*continued*).

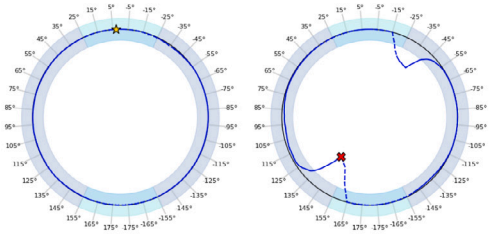

(s) o_{19}^{V}

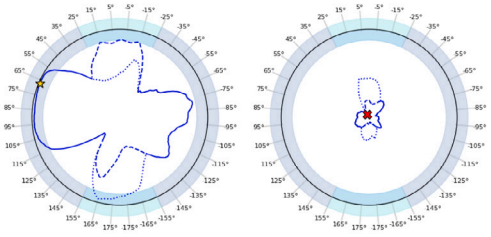

(t) o_{20}^{V}

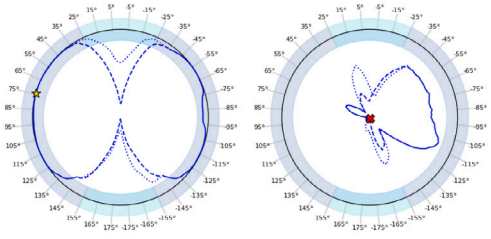

(u) o_{21}^{V}

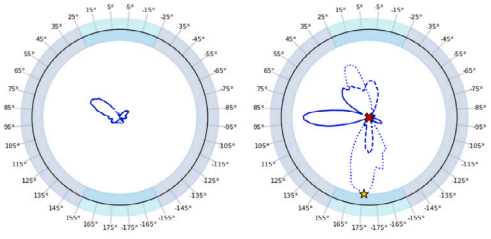

(v) o_{22}^{V}

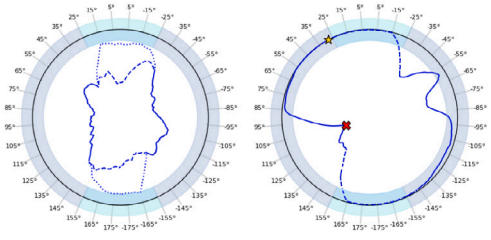

(w) o_{23}^{V}

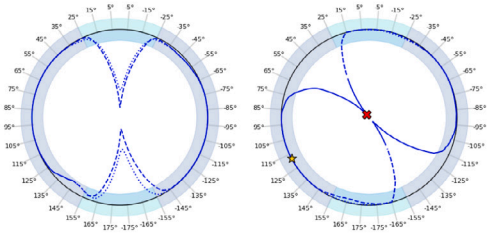

(x) o_{24}^{V}

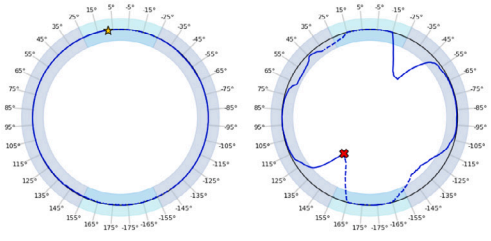

(y) o_{25}^{V}

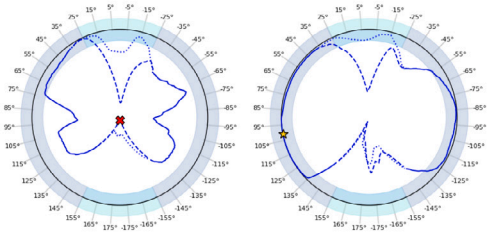

(z) o_{26}^{V}

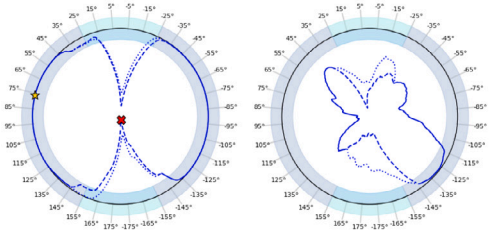

(aa) o_{27}^{V}

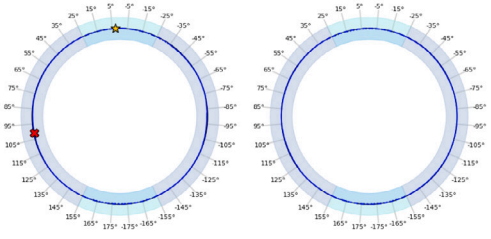

(ab) o_{28}^{V}

Fig. C.18. (*continued*).

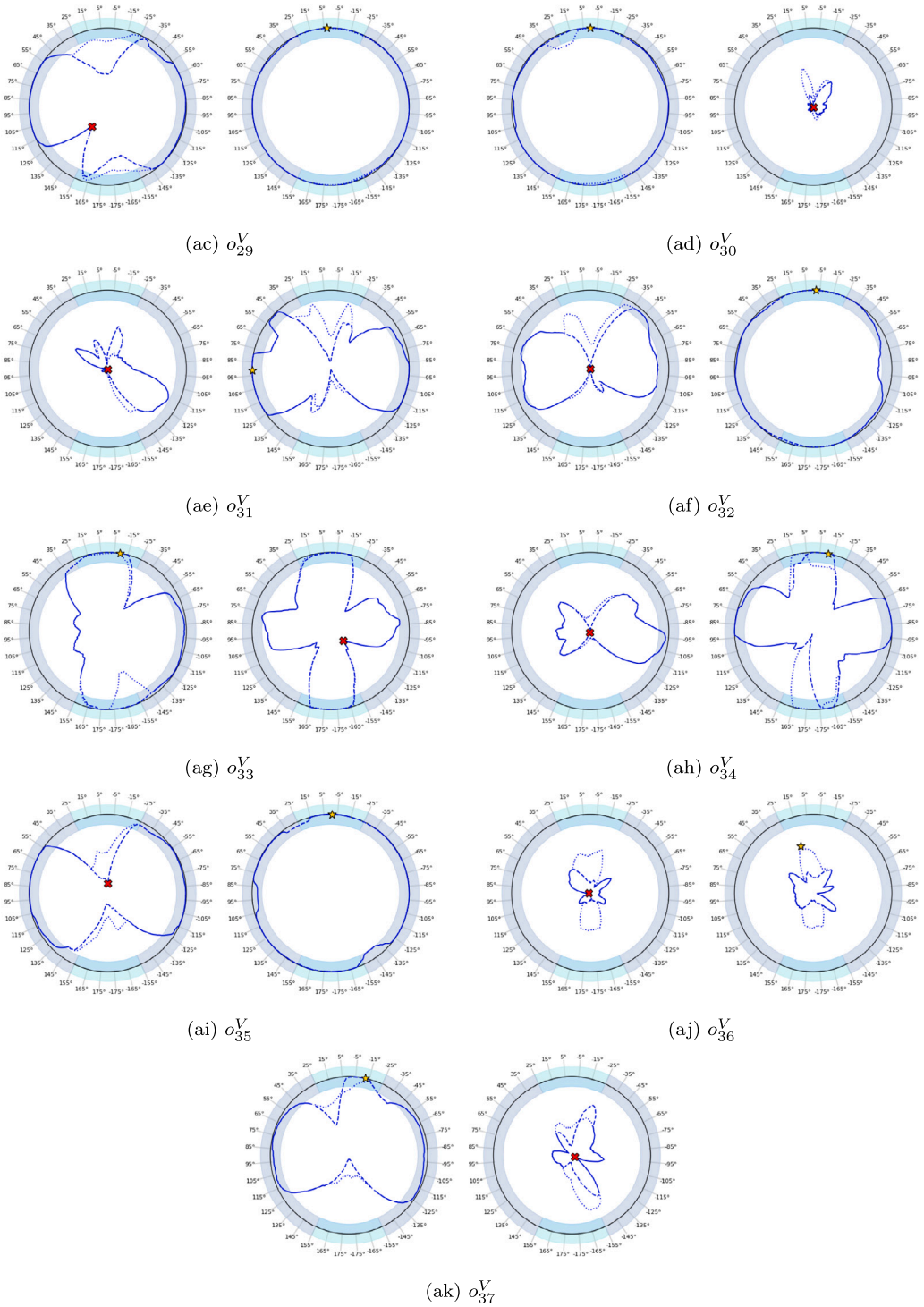

(ac) o_{29}^{V} (ad) o_{30}^{V}

(ae) o_{31}^{V} (af) o_{32}^{V}

(ag) o_{33}^{V} (ah) o_{34}^{V}

(ai) o_{35}^{V} (aj) o_{36}^{V}

(ak) o_{37}^{V}

Fig. C.18. (*continued*).

References

[1] S. Kadner, J. Kobus, E.G. Hansen, S. Akinci, P. Elsner, C. Hagelüken, M. Jaeger-Erben, M. Kick, A. Kwade, T. Müller-Kirschbaum, C. Kühl, D. Obeth, K. Schweitzer, M. Stuchtey, T. Vahle, T. Weber, P. Wiedemann, H. Wilts, R. Wittken, Circular Economy Roadmap for Germany, Tech. Rep., Acatech - Deutsche Akademie der Technikwissenschaften, 2021, http://dx.doi.org/10.48669/ceid_2021-4.

[2] N. Nasr, M. Thurston, Remanufacturing: A key enabler to sustainable product systems, Rochester Inst. Technol. 23 (2006).

[3] DIN SPEC 91472:2023-06, Remanufacturing (Reman) - Qualitätsklassifizierung für Zirkuläre Prozesse, Beuth Verlag GmbH, Berlin, 2023, http://dx.doi.org/10.31030/3434252, URL https://www.beuth.de/de/-/-/367509951.

[4] V.R. Guide, Production planning and control for remanufacturing: industry practice and research needs, J. Oper. Manage. 18 (4) (2000) 467–483, http://dx.doi.org/10.1016/S0272-6963(00)00034-6.

[5] J. Kurilova-Palisaitiene, E. Sundin, B. Poksinska, Remanufacturing challenges and possible lean improvements, J. Clean. Prod. 172 (2018) 3225–3236, http://dx.doi.org/10.1016/j.jclepro.2017.11.023.

[6] S. Yang, M.R. Aravind, J. Kaminski, H. Pepin, Opportunities for industry 4.0 to support remanufacturing, Appl. Sci. 8 (7) (2018) 1177, http://dx.doi.org/10.3390/app8071177.

[7] M. Kerin, D.T. Pham, A review of emerging industry 4.0 technologies in remanufacturing, J. Clean. Prod. 237 (2019) http://dx.doi.org/10.1016/j.jclepro.2019.117805.

[8] E.L.S. Teixeira, B. Tjahjono, M. Beltran, J. Julião, Demystifying the digital transition of remanufacturing: A systematic review of literature, Comput. Ind. 134 (2022) 103567, http://dx.doi.org/10.1016/j.compind.2021.103567.
[9] D. Tiwari, J. Miscandlon, A. Tiwari, G.W. Jewell, A review of circular economy research for electric motors and the role of industry 4.0 technologies, Sustainability 13 (17) (2021) 9668, http://dx.doi.org/10.3390/su13179668.
[10] J.-F. Klein, Predictive Object Transfer in Remanufacturing: A Cyber-Physical Approach Using Digital Twins (Ph.D. thesis), Karlsruhe Institute Of Technology (KIT), 2025, http://dx.doi.org/10.5445/IR/1000180419.
[11] A. Kaiblinger, M. Woschank, State of the art and future directions of digital twins for production logistics: A systematic literature review, Appl. Sci. (2) (2022) 669, http://dx.doi.org/10.3390/app12020669.
[12] Y. Zhu, J. Cheng, Z. Liu, Q. Cheng, X. Zou, H. Xu, Y. Wang, F. Tao, Production logistics digital twins: Research profiling, application, challenges and opportunities, Robot. Comput.-Integr. Manuf. 84 (2023) 102592, http://dx.doi.org/10.1016/j.rcim.2023.102592.
[13] J.B. Hauge, M. Zafarzadeh, Y. Jeong, Y. Li, W.A. Khilji, M. Wiktorsson, Employing digital twins within production logistics, in: 2020 IEEE International Conference on Engineering, Technology and Innovation, ICE/ITMC, IEEE, 2020, pp. 1–8, http://dx.doi.org/10.1109/ICE/ITMC49519.2020.9198540.
[14] P. Staczek, J. Pizoń, W. Danilczuk, A. Gola, A digital twin approach for the improvement of an autonomous mobile robots (AMR's) operating environment—A case study, Sensors 21 (23) (2021) http://dx.doi.org/10.3390/s21237830.
[15] J. Vachálek, D. Šišmišová, P. Vašek, I. Fit'ka, J. Slovák, M. Šimovec, Design and implementation of universal cyber-physical model for testing logistic control algorithms of production line's digital twin by using color sensor, Sensors 21 (5) (2021) 1842, http://dx.doi.org/10.3390/s21051842.
[16] M. Glatt, C. Sinnwell, L. Yi, S. Donohoe, B. Ravani, J.C. Aurich, Modeling and implementation of a digital twin of material flows based on physics simulation, J. Manuf. Syst. 58 (2021) 231–245, http://dx.doi.org/10.1016/j.jmsy.2020.04.015.
[17] Y. Zheng, S. Yang, H. Cheng, An application framework of digital twin and its case study, J. Ambient. Intell. Humaniz. Comput. 10 (3) (2019) 1141–1153, http://dx.doi.org/10.1007/s12652-018-0911-3.
[18] J.-F. Klein, M. Wurster, N. Stricker, G. Lanza, K. Furmans, Towards ontology-based autonomous intralogistics for agile remanufacturing production systems, in: 2021 26th IEEE International Conference on Emerging Technologies and Factory Automation, ETFA, IEEE, 2021, pp. 1–7, http://dx.doi.org/10.1109/ETFA45728.2021.9613486.
[19] J.-F. Klein, K. Furmans, Digital twin architecture and sim-to-real gap analysis of a material transfer system in a remanufacturing environment, in: K. Mpofu, N. Sacks, O. Damm (Eds.), Procedia CIRP, vol. 120, Elsevier B.V., 2023, pp. 368–373.
[20] X. Wang, L. Wang, Digital twin-based WEEE recycling, recovery and remanufacturing in the background of Industry 4.0, Int. J. Prod. Res. 57 (12) (2019) 3892–3902.
[21] R. Rocca, P. Rosa, C. Sassanelli, L. Fumagalli, S. Terzi, Integrating virtual reality and digital twin in circular economy practices: A laboratory application case, Sustainability 12 (6) (2020).
[22] O. Tozanli, E. Kongar, S. Gupta, Evaluation of waste electronic product trade-in strategies in predictive twin disassembly systems in the era of blockchain, Sustainability 12 (13) (2020) http://dx.doi.org/10.3390/su12135416.
[23] Y. Wang, S. Wang, B. Yang, L. Zhu, F. Liu, Big data driven hierarchical digital twin predictive remanufacturing paradigm: Architecture, control mechanism, application scenario and benefits, J. Clean. Prod. 248 (2020) http://dx.doi.org/10.1016/j.jclepro.2019.119299.
[24] Z. Chen, L. Huang, Digital twins for information-sharing in remanufacturing supply chain: A review, Energy 220 (2021) http://dx.doi.org/10.1016/j.energy.2020.119712.
[25] A. Shrivastava, S. Mukherjee, S. Chakraborty, Addressing the challenges in remanufacturing by laser-based material deposition techniques, Opt. Laser Technol. 144 (2021) http://dx.doi.org/10.1016/j.optlastec.2021.107404.
[26] Y. Yang, G. Yuan, J. Cai, S. Wei, Forecasting of disassembly waste generation under uncertainties using digital twinning-based hidden Markov model, Sustainability 13 (10) (2021) http://dx.doi.org/10.3390/su13105391.
[27] A. Zacharaki, T. Vafeiadis, N. Kolokas, A. Vaxevani, Y. Xu, M. Peschl, D. Ioannidis, D. Tzovaras, RECLAIM: Toward a new era of refurbishment and remanufacturing of industrial equipment, Front. Artif. Intell. 3 (2021) http://dx.doi.org/10.3389/frai.2020.570562.
[28] C. Assuad, T. Leirmo, K. Martinsen, Proposed framework for flexible de- and remanufacturing systems using cyber-physical systems, additive manufacturing, and digital twins, in: R. Teti, D. D'Addona (Eds.), Procedia CIRP, vol. 112, Elsevier B.V., 2022, pp. 226–231, http://dx.doi.org/10.1016/j.procir.2022.09.076.
[29] H. Ghorbani, F. Khameneifar, Construction of damage-free digital twin of damaged aero-engine blades for repair volume generation in remanufacturing, Robot. Comput.-Integr. Manuf. 77 (2022) http://dx.doi.org/10.1016/j.rcim.2022.102335.
[30] H.-F. Guo, Y. Han, Research on closed-loop supply chain based on digital twin, in: 2022 2nd International Conference on Algorithms, High Performance Computing and Artificial Intelligence, AHPCAI 2022, IEEE, 2022, pp. 270–273, http://dx.doi.org/10.1109/AHPCAI57455.2022.10087816.
[31] Y. Hu, C. Liu, M. Zhang, Y. Jia, Y. Xu, A conceptual framework of cyber-physical remanufacturing system, in: NanoMan 2022 and AETS 2022 - 2022 8th International Conference on Nanomanufacturing and 4th AET Symposium on ACSM and Digital Manufacturing, IEEE, 2022, pp. 1–6, http://dx.doi.org/10.1109/Nanoman-AETS56035.2022.10119511.
[32] G. Lanza, T. Asfour, J. Beyerer, B. Deml, J. Fleischer, M. Heizmann, K. Furmans, C. Hofmann, A. Cebulla, C. Dreher, J.-P. Kaiser, J.-F. Klein, F. Leven, S. Mangold, N. Mitschke, N. Stricker, J. Pfrommer, C. Wu, M. Wurster, M. Zaremski, Agiles produktionssystem mittels lernender roboter bei ungewissen produktzuständen am beispiel der anlasser-demontage, At - Autom. 70 (6) (2022) 504–516, http://dx.doi.org/10.1515/auto-2021-0158.
[33] S. Wiesner, L. Egbert, A. Zitnikov, Using operational data to represent machine components health and derive data-driven services, IFIP Adv. Inf. Commun. Technol. 664 IFIP (2022) http://dx.doi.org/10.1007/978-3-031-16411-8_35.
[34] J. Elsner, A. Gabriel, T. Ackermann, J. Körkemeyer, R. Schmitt, Digital twin-based life cycle assessment [auf digitalen zwillingen basiertes life cycle assessment integration des digitalen zwillings für die dynamische ökobilanzierung im variantenreichen remanufacturing von batterien], ZWF Z. Fuer Wirtsch. Fabr. 118 (12) (2023) 883–887, http://dx.doi.org/10.1515/zwf-2023-1167.
[35] C. Ke, X. Pan, P. Wan, Z. Huang, Z. Jiang, An intelligent redesign method for used products based on digital twin, Sustainability 15 (12) (2023) http://dx.doi.org/10.3390/su15129702.
[36] M. Kerin, N. Hartono, D. Pham, Optimising remanufacturing decision-making using the bees algorithm in product digital twins, Sci. Rep. 13 (1) (2023) http://dx.doi.org/10.1038/s41598-023-27631-2.
[37] M. Kerin, D. Pham, J. Huang, J. Hadall, A generic asset model for implementing product digital twins in smart remanufacturing, Int. J. Adv. Manuf. Technol. 124 (9) (2023) 3021–3038, http://dx.doi.org/10.1007/s00170-022-09295-w.
[38] X. Sun, H. Yu, W. Solvang, A digital reverse logistics twin for improving sustainability in industry 5.0, IFIP Adv. Inf. Commun. Technol. 690 AICT (2023) http://dx.doi.org/10.1007/978-3-031-43666-6_19.
[39] S. Li, Y. You, P. Zheng, X. Wang, L. Wang, Mutual-cognition for proactive human–robot collaboration: A mixed reality-enabled visual reasoning-based method, IISE Trans. 56 (10) (2024) 1099–1111, http://dx.doi.org/10.1080/24725854.2024.2313647.
[40] NVIDIA Cooperation, NVIDIA isaac sim, 2024, https://developer.nvidia.com/isaac-sim. (Accessed 08 May 2024).
[41] M. Wurster, B. Häfner, D. Gauder, N. Stricker, G. Lanza, Fluid automation — A definition and an application in remanufacturing production systems, Procedia CIRP 97 (2021) 508–513, http://dx.doi.org/10.1016/j.procir.2020.05.267.
[42] J. Pfrommer, J.-F. Klein, M. Wurster, S. Rapp, P. Grauberger, G. Lanza, A. Albers, S. Matthiesen, J. Beyerer, An ontology for remanufacturing systems, At - Autom. 70 (6) (2022) 534–541, http://dx.doi.org/10.1515/auto-2021-0156.
[43] B. Zhou, J.-F. Klein, B. Wang, M. Hillemann, Semantic mapping and autonomous navigation for agile production system, in: 2023 IEEE 19th International Conference on Automation Science and Engineering, CASE, IEEE, 2023, pp. 1–6, http://dx.doi.org/10.1109/CASE56687.2023.10260623.
[44] M. Pati, U. Majumdar, A letter on belt conveyor system as a mode of transportation in industry, Int. J. Res. Eng. Sci. Manag. 3 (12) (2020) 75–79, http://dx.doi.org/10.47607/ijresm.2020.411.
[45] J.-P. Kaiser, S. Lang, M. Wurster, G. Lanza, A concept for autonomous quality control for core inspection in remanufacturing, Procedia CIRP 105 (2022) 374–379, http://dx.doi.org/10.1016/j.procir.2022.02.062.
[46] N. Patki, R. Wedge, K. Veeramachaneni, The synthetic data vault, in: 2016 IEEE International Conference on Data Science and Advanced Analytics, DSAA, 2016, pp. 399–410, http://dx.doi.org/10.1109/DSAA.2016.49.
[47] C.J. Clopper, E.S. Pearson, The use of confidence or fiducial limits illustrated in the case of the binomial, Biometrika 26 (4) (1934) 404–413, http://dx.doi.org/10.2307/2331986.
[48] L.A. Orawo, Confidence intervals for the binomial proportion: A comparison of four methods, Open J. Stat. 11 (5) (2021) 806–816, http://dx.doi.org/10.4236/ojs.2021.115047.
[49] R.G. Newcombe, Interval estimation for the difference between independent proportions: comparison of eleven methods, Stat. Med. 17 (8) (1998) 873–890, http://dx.doi.org/10.1002/(sici)1097-0258(19980430)17:8<873::aid-sim779>3.0.co;2-i.
[50] M.W. Fagerland, S. Lydersen, P. Laake, Recommended confidence intervals for two independent binomial proportions, Stat. Methods Med. Res. 24 (2) (2015) 224–254, http://dx.doi.org/10.1177/0962280211415469.